

# Probabilistic Richardson Extrapolation

Chris. J. Oates<sup>1</sup>, Toni Karvonen<sup>2</sup>, Aretha L. Teckentrup<sup>3</sup>  
 Marina Strocchi<sup>4,5</sup>, Steven A. Niederer<sup>4,5,6</sup>

<sup>1</sup> School of Mathematics, Statistics and Physics, Newcastle University, UK

<sup>2</sup> Department of Mathematics and Statistics, University of Helsinki, FI

<sup>3</sup> School of Mathematics and Maxwell Institute for Mathematical Sciences, University of Edinburgh, UK

<sup>4</sup> National Heart and Lung Institute, Imperial College London, UK

<sup>5</sup> School of Biomedical Engineering and Imaging Sciences, King's College London, UK

<sup>6</sup> The Alan Turing Institute, UK

January 17, 2024

## Abstract

For over a century, extrapolation methods have provided a powerful tool to improve the convergence order of a numerical method. However, these tools are not well-suited to modern computer codes, where multiple continua are discretised and convergence orders are not easily analysed. To address this challenge we present a probabilistic perspective on Richardson extrapolation, a point of view that unifies classical extrapolation methods with modern multi-fidelity modelling, and handles uncertain convergence orders by allowing these to be statistically estimated. The approach is developed using Gaussian processes, leading to *Gauss–Richardson Extrapolation* (GRE). Conditions are established under which extrapolation using the conditional mean achieves a polynomial (or even an exponential) speed-up compared to the original numerical method. Further, the probabilistic formulation unlocks the possibility of experimental design, casting the selection of fidelities as a continuous optimisation problem which can then be (approximately) solved. A case-study involving a computational cardiac model demonstrates that practical gains in accuracy can be achieved using the GRE method.

## 1 Introduction

Testing of hypotheses underpins the scientific method, and increasingly these hypotheses are model-based. Deterministic or stochastic mathematical models are routinely used to represent mechanisms hypothesised to govern diverse phenomena, such as aerodynamics or electrochemical regulation of the human heart. In these cases, critical scientific enquiry

demands a comparison of the model against a real-world dataset. The practical challenge is two-fold; to simulate from the mathematical model, and to obtain a real-world dataset. Here we focus on the first challenge – simulating from the model – which can be arbitrarily difficult depending on the complexity of the model. For example, simulating a single cycle of a jet engine to an acceptable numerical precision routinely requires  $10^6$  core hours (Arroyo et al., 2021), while accurate simulation from the cardiac models that we consider later in this paper at steady state requires  $10^4$  core hours in total (Strocchi et al., 2023). To drive progress in these, and many other diverse scientific domains, there is an urgent need for statistical and computational methodology that can mitigate the high cost of accurately simulating from a mathematical model.

Abstractly, we enumerate all of the *discretisation parameters* involved in approximate simulation from the mathematical model using scalars  $\mathbf{x} = (x_1, \dots, x_d)$ , such that each component of  $\mathbf{x}$  controls the error due to a particular aspect of discretisation; for example,  $x_1$  could be a time step size,  $x_2$  could be the width of a spatial mesh, and  $x_3$  could be an error tolerance for an adaptive numerical method. The principal requirement is that the ideal mathematical model corresponds to the limit  $\mathbf{x} \rightarrow \mathbf{0}$  where no discretisation is performed. Given a value of  $\mathbf{x}$ , we denote as  $f(\mathbf{x})$  the associated numerical approximation to the continuum quantity  $f(\mathbf{0})$  from the mathematical model. The computational cost of such an evaluation will be denoted  $c(\mathbf{x})$ , with  $c(\mathbf{0}) = \infty$  being typical. The computational challenge addressed in this paper is to produce an accurate approximation to  $f(\mathbf{0})$ , based on a dataset of simulations  $\{f(\mathbf{x}_j)\}$ , where  $\{\mathbf{x}_j\} \subset (0, \infty)^d$ , such that the computational cost of obtaining  $\{f(\mathbf{x}_j)\}$  remains within a prescribed budget. For this initial discussion we focus on scalar-valued model output, but we generalise to multivariate and infinite-dimensional model output in Section 2.9.

Several solutions have been proposed to perform approximate simulation at reduced cost. In what follows it is useful to draw a distinction between *extrapolation methods*, applicable to the situation where a mathematical model is discretised for simulation and numerical analysis of the discretisation error can be performed, and *modern solutions* that are typically applied to ‘black box’ computer codes for which numerical analysis is impractical.

**Extrapolation Methods** A unified presentation of extrapolation methods, that includes the most widely-used algorithms, is provided by the so-called *E-algorithm* (see the survey of Brezinski, 1989). The starting point is a (real-valued) convergent sequence, which in our setting we interpret as a sequence of numerical approximations  $(f(\mathbf{x}_m))_{m \in \mathbb{N}}$ , where  $\mathbf{x}_m$  is a vector of discretisation parameters controlling the error in approximating the mathematical model, while  $f(\mathbf{0})$  represents the continuum quantity of interest. The E-algorithm posits an *ansatz* that

$$f(\mathbf{x}_m) = f(\mathbf{0}) + a_1 g_1(m) + \dots + a_{n-1} g_{n-1}(m) \tag{1}$$

for some unknown  $a_1, \dots, a_{n-1} \in \mathbb{R}$ , some known functions  $g_i : \mathbb{N} \rightarrow \mathbb{R}$ , and all  $m \in \mathbb{N}$ . Then, instantiating (1) for  $m, m+1, \dots, m+n-1$ , we may solve for the unknown  $a_1, \dots, a_{n-1}$  and  $f(\mathbf{0})$  in terms of the  $n$  values  $f(\mathbf{x}_m), \dots, f(\mathbf{x}_{m+n-1})$ . Indeed, solving this linear system for

$f(\mathbf{0})$  leads to the estimator

$$S_m := S(f(\mathbf{x}_m), \dots, f(\mathbf{x}_{m+n-1})) = \frac{\begin{vmatrix} f(\mathbf{x}_m) & \dots & f(\mathbf{x}_{m+n-1}) \\ g_1(m) & \dots & g_1(m+n-1) \\ \vdots & & \vdots \\ g_n(m) & \dots & g_n(m+n-1) \end{vmatrix}}{\begin{vmatrix} 1 & \dots & 1 \\ g_1(m) & \dots & g_1(m+n-1) \\ \vdots & & \vdots \\ g_n(m) & \dots & g_n(m+n-1) \end{vmatrix}}. \quad (2)$$

Under appropriate assumptions, the sequence  $(S_m)_{m \in \mathbb{N}}$  constructed based on  $(f(\mathbf{x}_m))_{m \in \mathbb{N}}$  as in (2) not only has the same limit,  $f(\mathbf{0})$ , but also converges to that limit faster in the sense that  $\lim_{m \rightarrow \infty} (S_m - f(\mathbf{0})) / (f(\mathbf{x}_m) - f(\mathbf{0})) = 0$ ; for precise statements see Chapter 2 of Brezinski and Zaglia (2013).

The principal classes of extrapolation methods concern either the case of a single discretisation parameter  $x_m$ , or they maintain ambivalence about  $\mathbf{x}_m$  by operating only on the values of the sequence  $(f(\mathbf{x}_m))_{m \in \mathbb{N}}$ . In either case, different extrapolation methods correspond to different basis functions  $g_i$  in (1). *Richardson extrapolation* corresponds to  $g_i(m) = x_m^i$ , in which case (1) is recognised as polynomial extrapolation to the origin (Richardson, 1911; Richardson and Gaunt, 1927). The existence of a Taylor expansion of  $f$  at the origin is sufficient to guarantee a polynomial-rate convergence acceleration using Richardson’s method. Other examples of extrapolation methods include *Shanks’ transformation*  $g_i(m) = f(\mathbf{x}_{m+i}) - f(\mathbf{x}_{m+i-1})$  (Shanks, 1955), the *Germain–Bonne transformation*  $g_i(m) = (f(\mathbf{x}_{m+1}) - f(\mathbf{x}_m))^i$  (Germain-Bonne, 1990), and *Thiele’s rational extrapolation method*  $g_i(m) = x_m^i$ ,  $g_{i+p}(m) = f(x_m)x_m^i$  for  $i = 1, \dots, p$ ,  $n = 2p + 1$  (Thiele, 1909; Buirsch and Stoer, 1964; Larkin, 1967). A careful numerical analysis of  $f$  is usually required to determine when a particular extrapolation method can be applied. To the best of our knowledge, ideas from statistics and uncertainty quantification do not feature prominently, if at all, in the literature on extrapolation methods. In addition, the question of how best to construct the sequence  $(\mathbf{x}_m)_{m \in \mathbb{N}}$  under a constraint on the overall computational budget does not appear to have been systematically addressed. Further background can be found in the book-level treatment of Sidi (2003) and Brezinski and Zaglia (2013).

Though rather classical, extrapolation methods continue to find new and useful applications, including in optimal transport (Chizat et al., 2020), regularisation and training of machine learning models (Bach, 2021), and sampling with Markov chain Monte Carlo (Durmus et al., 2016).

**Modern Solutions** If the mathematical model additionally involves one or more degrees of freedom  $\boldsymbol{\theta}$ , numerical approximations  $f_{\boldsymbol{\theta}}(\mathbf{x})$  are often required across a range of values for  $\boldsymbol{\theta}$  to identify configurations that are consistent with observations from the real world. Since the introduction of additional degrees of freedom further complicates numerical analysis, this

setting has motivated the development of black box methods that can be applied in situations where numerical analysis is impractical. Among these, *emulation* and *multi-fidelity modelling* are arguably the most prominent.

In *emulation* one attempts to approximate the map  $\boldsymbol{\theta} \mapsto f_{\boldsymbol{\theta}}(\mathbf{x}_{\text{hi-fi}})$ , where the discretisation parameters  $\mathbf{x}_{\text{hi-fi}}$  are typically fixed and correspond to a suitably *high fidelity* (hi-fi) model. This enables prediction of computer code output at values of  $\boldsymbol{\theta}$  for which simulation was not performed (Sacks et al., 1989). A variety of sophisticated techniques have been developed to identify an appropriate basis or subspace in which an emulator can be constructed, such as *reduced order modelling* (Lucia et al., 2004). One drawback of emulation is that it can be *data hungry*; in applications for which it is only possible to perform a small number  $n$  of simulations, and for which insight from numerical analysis is unavailable, one usually cannot expect to obtain high-quality predictions. A second drawback is that emulation treats the discretised model  $\boldsymbol{\theta} \mapsto f_{\boldsymbol{\theta}}(\mathbf{x}_{\text{hi-fi}})$  as the target, whereas in reality the continuum mathematical model  $\boldsymbol{\theta} \mapsto f_{\boldsymbol{\theta}}(\mathbf{0})$  is of principal interest.

A partial solution to the drawbacks of emulation is *multi-fidelity modelling* (MFM), in which one supplements a small number of simulations from the hi-fi model  $\boldsymbol{\theta} \mapsto f_{\boldsymbol{\theta}}(\mathbf{x}_{\text{hi-fi}})$  with a larger number of simulations from one or more cheaper *low fidelity* (lo-fi) models  $\boldsymbol{\theta} \mapsto f_{\boldsymbol{\theta}}(\mathbf{x}_{\text{lo-fi}})$  (Peherstorfer et al., 2018). Lo-fi models can sometimes be obtained using coarse-grid approximations, early stopping of iterative algorithms, or linearisation (Piperni et al., 2013). Alternatively, lo-fi models could involve only a subset of the relevant physical mechanisms, an approach popular e.g. in climate science (Held, 2005; Majda and Gershgorin, 2010). Once specified, the models of different fidelities can be combined in different ways: one can either use the hi-fi model to periodically ‘check’ (and possibly adapt) the lo-fi models; or one can use the lo-fi models as pilot runs to decide whether or not to evaluate the hi-fi model; or one can use the information from all models simultaneously, by defining a multi-fidelity surrogate model (Craig et al., 1998; Kennedy and O’Hagan, 2000; Cumming and Goldstein, 2009; Ehara and Guillas, 2023) where correlation between models is taken into account. Provided that the lo-fi models are correlated with the original model, these additional cheap simulations can be leveraged to more accurately predict computer code output. The principal drawback of multi-fidelity modelling is that there is limited guidance on how the lo-fi models should be constructed, and a poor choice can fail to improve (or even worsen) predictive performance, whilst incurring an additional computational cost. In addition, as with emulation, the literature on MFM tends to treat the hi-fi model as the target, rather than the continuum mathematical model.

**Other Related Work** Some alternative lines of research will briefly be discussed. *Probabilistic numerics* casts numerical approximation as a statistical task (Hennig et al., 2015), with Bayesian principles used to quantify uncertainty regarding the continuum model of interest (Cockayne et al., 2019). However, the focus of that literature is the design of numerical methods, in contrast to extrapolation methods which operate on the output of existing numerical methods. In parallel, the application of machine learning methods to numerical tasks has received recent attention; for example deep learning is being used for numeri-

cal approximation of high-dimensional parametric partial differential equations (Han et al., 2018). This literature does not attempt extrapolation as such, with a hi-fi numerical method typically used to provide a training dataset. Gaussian processes have been used in specific applications to extrapolate a series of numerical approximations to a continuum quantity of interest  $f(\mathbf{0})$ , for example in Thodoroff et al. (2023) to model ice sheets in Antarctic, and in Ji et al. (2022) to model the evolution of the quark-gluon plasma following the Big Bang. To date, however, convergence acceleration has not been studied in the Gaussian process context. An important numerical task encountered in statistics is to approximate an expected value of interest  $f(\mathbf{0}) = \mathbb{E}[X(\mathbf{0})]$ . Unbiased estimation of  $f(\mathbf{0})$  at finite cost is possible in this setting using the methodology of Rhee and Glynn (2015), provided one can construct a sequence  $(X(\mathbf{x}_n))_{n \in \mathbb{N}}$  of computable stochastic approximations to  $X(\mathbf{0})$ , such that the variance of  $X(\mathbf{x}_n) - X(\mathbf{x}_{n-1})$  decays sufficiently fast. Similar de-biasing ideas have since been used in the context of Markov chain Monte Carlo (Jacob et al., 2020). Multilevel methods, based on such sequences, have been combined with Richardson extrapolation in Lemaire and Pagès (2017); Beschle and Barth (2023).

**Our Contribution** This paper proposes a probabilistic perspective on extrapolation methods that unifies extrapolation methods and MFM. The approach is instantiated using a *numerical analysis-informed Gaussian process* to approximate the map  $\mathbf{x} \mapsto f(\mathbf{x})$ , as described in Section 2, where the conditional mean can be interpreted as a (novel) extrapolation method, in the sense that it provably achieves a polynomial (or even an exponential) speed-up compared to the original numerical method. Like Richardson extrapolation, our theoretical arguments are rooted in Taylor expansions, so the name *Gauss–Richardson Extrapolation* (GRE) is adopted. The probabilistic formulation of extrapolation methods confers several advantages:

- In contrast to classical extrapolation methods, which focus on the case of a univariate discretisation parameter  $x_n$ , it is straight-forward to consider a vector of discretisation parameters  $\mathbf{x}_n$  within a regression framework. In Sections 2.1 to 2.3 the probabilistic approach is laid out, then in Sections 2.4 and 2.5 higher-order convergence guarantees for GRE are established.
- Credible sets for the continuum quantity of interest  $f(\mathbf{0})$  can be constructed, enabling computational uncertainty to be integrated into experimental design and downstream decision-support. The asymptotic performance of GRE credible sets is analysed in Section 2.6.
- In contrast to existing approaches in MFM, where a discrete set of fidelities are specified at the outset, GRE operates on a continuous spectrum of fidelities and casts the selection of fidelities as a cost-constrained experimental design problem, which can then be approximately solved using methods described in Section 2.7.
- For computer models whose convergence order is difficult to analyse, the probabilistic formulation allows for convergence orders to be formally estimated. The consistency

of a maximum quasi-likelihood approach to estimating unknown convergence order is established in Section 2.8.

The methodology is rigorously tested in the context of simulating from a computational cardiac model involving separate spatial and temporal discretisation parameters in Section 3. The sensitivity of the cardiac model to the different discretisation parameters is first estimated from lo-fi simulations, then an optimal experimental design is generated and used to estimate the true trajectory of the cardiac model in the continuum limit. Our experimental results demonstrate that a practical gain in accuracy can be achieved with our GRE method. Though our assessment focuses on a specific cardiac model of scientific and clinical interest, the methodology is general and offers an exciting possibility to accelerate computation in the diverse range of scenarios in which computationally-intensive simulation is performed. A closing discussion is contained in Section 4.

## 2 Methodology

This section presents a novel probabilistic perspective on extrapolation methods, which we instantiate using *Gaussian processes* (GPs) to produce methodology that we term *Gauss–Richardson Extrapolation* (GRE). For simplicity of presentation, we first consider the case of a scalar quantity of interest, generalising to arbitrary-dimensional quantities of interest in Section 2.9.

**Set-Up** Let  $f : \mathcal{X} \rightarrow \mathbb{R}$  be a (non-random) real-valued function on a bounded set  $\mathcal{X} \subset [0, \infty)^d$  such that  $\mathbf{0} \in \mathcal{X}$ . As we explained in Section 1, the output  $f(\mathbf{x})$  for  $\mathbf{x} \neq \mathbf{0}$  will represent a numerical approximation to a continuum quantity  $f(\mathbf{0})$  of interest, and for extrapolation to be possible at all we will minimally need to assume that  $f$  is continuous at  $\mathbf{0}$ .

**Notation** For  $\boldsymbol{\beta} \in \mathbb{N}_0^p$ , let  $\partial^{\boldsymbol{\beta}}g$  denote the mixed partial derivative  $\mathbf{x} \mapsto \partial_{x_1}^{\beta_1} \dots \partial_{x_p}^{\beta_p} g(\mathbf{x})$  of a function  $g : D \rightarrow \mathbb{R}$ , whenever this is well-defined and  $D \subseteq \mathbb{R}^p$ . Let  $C^s(D)$  denote the set of  $s$ -times continuously differentiable functions  $g : D \rightarrow \mathbb{R}$ , meaning that  $\partial^{\boldsymbol{\beta}}g$  is continuous for all  $|\boldsymbol{\beta}| \leq s$ , where  $|\boldsymbol{\beta}| := \beta_1 + \dots + \beta_p$ . For  $g : D \rightarrow \mathbb{R}$  bounded, let  $\|g\|_{L^\infty(D)} := \sup_{\mathbf{x} \in D} |g(\mathbf{x})|$ . Let  $\pi_r(D)$  denote the set of all polynomial functions of total degree at most  $r$  on  $D$ . For vectors  $\mathbf{a}, \mathbf{b} \in \mathbb{R}^d$ , let  $[\mathbf{a}, \mathbf{b}] := [a_1, b_1] \times \dots \times [a_d, b_d] \subset \mathbb{R}^d$ , and similarly for  $[\mathbf{a}, \mathbf{b}]$  and so forth. Let  $\mathcal{GP}(m, k)$  denote the law of a GP with mean function  $m$  and covariance function  $k$ ; background on GPs can be found in Rasmussen and Williams (2006).

### 2.1 A Numerical Analysis-Informed Gaussian Process

Assuming for the moment that numerical analysis of  $\mathbf{x} \mapsto f(\mathbf{x})$  can be performed, our first aim is to encode the resulting bounds on discretisation error into a statistical regression model. Training such a *numerical analysis-informed* regression model on data  $\{f(\mathbf{x}_i)\}_{i=1}^n$

obtained at distinct inputs  $X_n = \{\mathbf{x}_i\}_{i=1}^n \subset \mathcal{X} \setminus \{\mathbf{0}\}$  enables statistical prediction of the limit  $f(\mathbf{0})$ , in analogy with classical extrapolation methods. To leverage conjugate computation, here we instantiate the idea using GPs in a Bayesian framework. For the first part, we require an explicit error bound  $b : \mathcal{X} \rightarrow [0, \infty)$  such that  $b(\mathbf{x}) \geq 0$  with equality if and only if  $\mathbf{x} = \mathbf{0}$ , and such that  $f(\mathbf{x}) - f(\mathbf{0}) = O(b(\mathbf{x}))$ . The error bound  $b$  will be encoded into a centred prior GP model for  $f$ , whose covariance function

$$k(\mathbf{x}, \mathbf{x}') := \sigma^2 [k_0^2 + b(\mathbf{x})b(\mathbf{x}')k_e(\mathbf{x}, \mathbf{x}')], \quad \mathbf{x}, \mathbf{x}' \in \mathcal{X}, \quad (3)$$

is selected to ensure samples  $g \sim \mathcal{GP}(0, k)$  from the GP satisfy, with probability one,  $g(\mathbf{x}) - g(\mathbf{0}) = O(b(\mathbf{x}))$  (see Appendix B.1 for the precise statement). Here  $\sigma^2 > 0$  is an overall scale to be estimated, while the scalar  $k_0^2 > 0$  is proportional to the prior variance of  $f(\mathbf{0})$ . The symmetric positive-definite function  $k_e : \mathcal{X} \times \mathcal{X} \rightarrow \mathbb{R}$  is the covariance function for the *normalised error*  $\mathbf{x} \mapsto e(\mathbf{x})$ , where  $e(\mathbf{x}) := b(\mathbf{x})^{-1}(f(\mathbf{x}) - f(\mathbf{0}))$  for  $\mathbf{x} \in \mathcal{X} \setminus \{\mathbf{0}\}$ , and must be specified. In practice  $k_e$  will additionally involve length-scale parameters  $\ell$  which must be estimated, for example  $k_e(\mathbf{x}, \mathbf{x}') = \exp(-\sum_{i=1}^d \ell_i^{-2}(x_i - x'_i)^2)$  in the case of the Gaussian kernel; we defer all discussion of this point to Sections 2.8 and 3. To our knowledge, the encoding of convergence orders into a GP as in (3) has not been well-studied, though the basic idea appeared in Tuo et al. (2014) and in our preliminary work (Teymur et al., 2021). Standard techniques can be applied to fit such a GP model to a dataset; see Figure 1 and Section 2.2.

**Remark 1** (Recovering Richardson in dimension  $d = 1$ ). *Let  $k_e$  be any kernel that reproduces the polynomial space  $\pi_{n-2}(\mathbb{R})$ , such as  $k_e(x, x') = (1 + xx')^{n-2}$ , and consider the ‘objective’ prior with  $k_0^2 \rightarrow \infty$ . Conditioning on data  $\{f(x_i)\}_{i=1}^n$ , the posterior mean function is the unique interpolant of the form  $x \mapsto \mu + b(x)p(x)$  for some  $\mu \in \mathbb{R}$ ,  $p \in \pi_{n-2}(\mathbb{R})$  (see e.g. Karvonen et al., 2018, Proposition 2.6). Thus, if  $b$  is polynomial, the intercept  $\mu$  is the result of polynomial extrapolation to 0, and is an instance of Richardson’s classical extrapolation method.*

Unfortunately the connection in Remark 1 is not especially useful. Indeed, while the posterior mean provides a useful point estimate, the posterior variance is identically zero, meaning that predictive uncertainty is not being properly quantified. Thus we do not attempt to reproduce Richardson extrapolation in the sequel, but rather we develop *de novo* methodology tailored to the GP framework.

## 2.2 Gauss–Richardson Extrapolation

First we recall the relevant calculations for conditioning the GP model (3) on a dataset. Let  $k_b : \mathcal{X} \times \mathcal{X} \rightarrow \mathbb{R}$  be defined as  $k_b(\mathbf{x}, \mathbf{x}') := b(\mathbf{x})b(\mathbf{x}')k_e(\mathbf{x}, \mathbf{x}')$ , so that our assumptions on  $b$  and  $k_e$  imply that  $k_b$  is a symmetric positive-definite kernel on  $\mathcal{X} \setminus \{\mathbf{0}\}$ , and a symmetric positive semi-definite kernel on  $\mathcal{X}$ . Let  $f(X_n)$  be a column vector with entries  $f(\mathbf{x}_i)$ , let  $\mathbf{k}_b(\mathbf{x})$  be a column vector with entries  $k_b(\mathbf{x}_i, \mathbf{x})$ , and let  $\mathbf{K}_b$  be a matrix with entries  $k_b(\mathbf{x}_i, \mathbf{x}_j)$ . Recalling that  $k_0^2$  is proportional to the prior variance for  $f(\mathbf{0})$ , we opt for an ‘objective’ prior in which

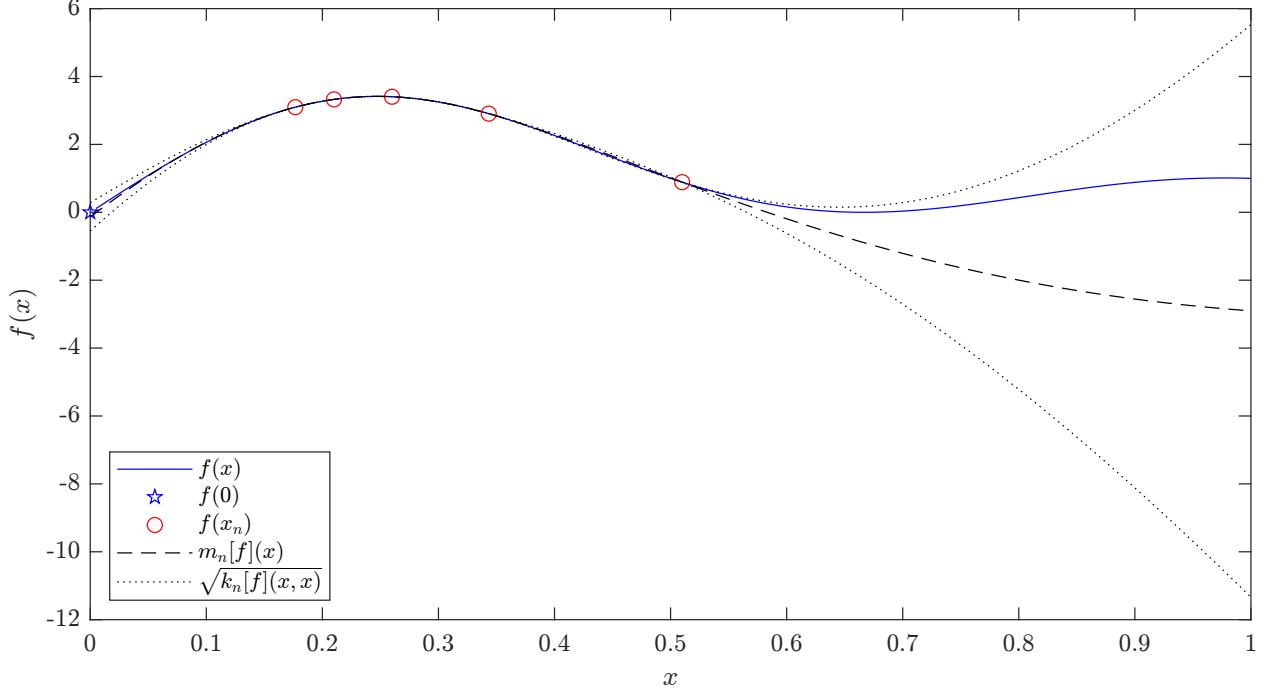


Figure 1: The numerical analysis-informed Gaussian process model, fitted to an illustrative dataset  $\{f(x_i)\}_{i=1}^n$  (red circles) of size  $n = 5$ , corresponding to the approximations produced by a finite difference method (blue solid curve) whose first-order accuracy [i.e.,  $b(x) = x$ ] was encoded into the GP. The scale  $\sigma_n^2[f]$  of the uncertainty was calibrated using the method advocated in Section 2.6, while  $k_e$  was taken to be a Matérn- $\frac{5}{2}$  kernel with length-scale parameter selected using quasi maximum likelihood likelihood (see Section 2.8). Observe that point estimate  $m_n[f](0)$  (black dashed curve at  $x = 0$ ), is more accurate than that of the highest fidelity simulation from the numerical method, while the limiting quantity of interest  $f(0)$  (blue star) falls within the one standard deviation prediction interval (black dotted curves at  $x = 0$ ).

$k_0^2 \rightarrow \infty$ . However, this limit results in an improper prior GP. To make progress, we must first compute the conditional GP using a finite value of  $k_0^2$  and then retrospectively take the limit – a standard calculation which we detail in Appendix B.2 – yielding conditional mean and covariance functions

$$m_n[f](\mathbf{x}) := \frac{\mathbf{1}^\top \mathbf{K}_b^{-1} f(X_n)}{\mathbf{1}^\top \mathbf{K}_b^{-1} \mathbf{1}} + \mathbf{k}_b(\mathbf{x})^\top \mathbf{K}_b^{-1} \left\{ f(X_n) - \left( \frac{\mathbf{1}^\top \mathbf{K}_b^{-1} f(X_n)}{\mathbf{1}^\top \mathbf{K}_b^{-1} \mathbf{1}} \right) \mathbf{1} \right\}, \quad (4)$$

$$k_n[f](\mathbf{x}, \mathbf{x}') := \sigma_n^2[f] \left\{ k_b(\mathbf{x}, \mathbf{x}') - \mathbf{k}_b(\mathbf{x})^\top \mathbf{K}_b^{-1} \mathbf{k}_b(\mathbf{x}') + \frac{[\mathbf{k}_b(\mathbf{x})^\top \mathbf{K}_b^{-1} \mathbf{1} - 1][\mathbf{k}_b(\mathbf{x}')^\top \mathbf{K}_b^{-1} \mathbf{1} - 1]}{\mathbf{1}^\top \mathbf{K}_b^{-1} \mathbf{1}} \right\}, \quad (5)$$

where  $\mathbf{1}$  is a column vector whose elements are all 1. The matrix  $\mathbf{K}_b$  can indeed be inverted since we have assumed that the entries of  $X_n \subset \mathcal{X} \setminus \{\mathbf{0}\}$  are distinct. To obtain (5) we have



additionally replaced  $\sigma^2$  with  $\sigma_n^2[f]$ , an estimator for the scale parameter  $\sigma$ , to be specified in Section 2.6. Computing the conditional mean and variance at  $\mathbf{x} = \mathbf{0}$  results in the simple formulae

$$m_n[f](\mathbf{0}) = \frac{\mathbf{1}^\top \mathbf{K}_b^{-1} f(X_n)}{\mathbf{1}^\top \mathbf{K}_b^{-1} \mathbf{1}} \quad \text{and} \quad k_n[f](\mathbf{0}, \mathbf{0}) = \frac{\sigma_n^2[f]}{\mathbf{1}^\top \mathbf{K}_b^{-1} \mathbf{1}}, \quad (6)$$

since  $b(\mathbf{0}) = 0$ , and thus  $k_b(\mathbf{0}, \mathbf{x}) = b(\mathbf{0})b(\mathbf{x})k_e(\mathbf{0}, \mathbf{x}) = 0$  for all  $\mathbf{x} \in \mathcal{X}$ . The proposed GRE method returns a (univariate) Gaussian distribution, which can be summarised using the point estimate  $m_n[f](\mathbf{0})$  for  $f(\mathbf{0})$ , together with the  $100(1 - \alpha)\%$  credible intervals

$$C_\alpha[f] = \left\{ y \in \mathbb{R} : \frac{|y - m_n[f](\mathbf{0})|}{\sqrt{k_n[f](\mathbf{0}, \mathbf{0})}} \leq \Phi^{-1} \left( 1 - \frac{\alpha}{2} \right) \right\} \quad (7)$$

where  $\Phi$  denotes the standard Gaussian cumulative density function. The uncertainty quantification provided by GRE unlocks additional functionality that was not available to classical extrapolation methods, including optimal experimental design for selecting  $X_n$  (Section 2.7) and principled statistical methods for estimating uncertain convergence orders (Section 2.8). However, both the accuracy of the point estimate and the coverage of the credible intervals will depend critically on the choice of the scale estimator  $\sigma_n^2[f]$  and the choice of covariance function  $k_e$ . This important issue of how to select  $\sigma_n^2[f]$  and  $k_e$  will be discussed next. An illustration of the proposed GRE method is provided in Figure 1.

## 2.3 Conservative Gaussian Process Priors

Our set-up involves a non-random function  $f$  that is modelled using a prior GP. One would perhaps hope to elicit a prior covariance function  $k$  in such a manner that  $f$  could plausibly have been generated as a sample from the GP. However, such elicitation is fundamentally difficult; the sample support set of a GP is not a vector space and may not even be measurable in general (Stein and Hung, 2019; Karvonen, 2023). How then can we proceed? In the applications that we have in mind, it is often possible to identify a symmetric positive-definite kernel such that  $f$  belongs to the *reproducing kernel Hilbert space* (RKHS) associated to the kernel, whose elements are real-valued functions on  $\mathcal{X}$ . For example, in numerical analysis it is often possible to reason that  $f$  possesses a certain number of derivatives, from which inclusion in certain Sobolev RKHSs can be deduced. The approach that we take is to identify the covariance function  $k$  with the kernel of an RKHS, denoted  $\mathcal{H}_k(\mathcal{X})$ , in which  $f$  is contained. In particular, for any  $k_0^2 \in (0, \infty)$  the space reproduced by the kernel  $k$  in (3) consists of functions  $g : \mathcal{X} \rightarrow \mathbb{R}$  of the form  $g(\mathbf{x}) = \mu + b(\mathbf{x})e(\mathbf{x})$  where  $\mu \in \mathbb{R}$  and  $e \in \mathcal{H}_{k_e}(\mathcal{X})$ , and in the  $k_0^2 \rightarrow \infty$  limit the norm structure of  $\mathcal{H}_k(\mathcal{X})$  reduces to a seminorm  $|g|_{\mathcal{H}_k(\mathcal{X})} := \|\mathbf{x} \mapsto (g(\mathbf{x}) - g(\mathbf{0}))/b(\mathbf{0})\|_{\mathcal{H}_{k_e}(\mathcal{X})}$  induced by the norm structure of  $\mathcal{H}_{k_e}(\mathcal{X})$ ; further background on RKHS can be found in Berlinet and Thomas-Agnan (2011). This construction results in a *conservative* prior GP, since with probability one sample paths will be less regular than  $f$  when the RKHS is infinite-dimensional. However, there are several senses in which this approach to prior elicitation can be justified. First, it can be viewed as

a form of ‘objective’ prior for GPs, in the sense that it is not intended to reflect prior belief but is rather intended to induce desirable behaviour in the posterior GP. Second, the choices that we make here will be justified through theoretical guarantees on both point estimation error (Section 2.4) and coverage of credible sets (Section 2.6). Third, the introduction of an additional scale estimator  $\sigma_n^2[f]$  in (5) provides an opportunity to counteract the conservatism of the choice of  $k$  through the data-driven estimation of an appropriate scale for the credible sets in (7).

## 2.4 Higher-Order Convergence Guarantees

The main technical contribution of this paper is to establish sufficient conditions under which the GRE point estimate  $m_n[f](\mathbf{0})$  in (6) provides a more accurate approximation to the continuum limit  $f(\mathbf{0})$  compared to the highest fidelity approximation  $f(\mathbf{x}_n)$  on which it is based. The analysis we present is based on local polynomial reproduction, similar to that described in Wendland (2004). However, our results differ from existing work in that they are adapted to the non-stationary kernel (3) and quantify the space-filling properties of a design  $X_n$  using boxes, rather than balls or cones, since boxes are more natural for the domain  $\mathcal{X} \subseteq [0, \infty)^d$  and enable sharper control over the constants involved.

To state our results, we define the *box fill distance*  $\rho_{X_n, \mathcal{X}}$  as the supremum value of  $\nu$  such that there is a box of the form  $[\mathbf{x}, \mathbf{x} + \nu \mathbf{1}]$  contained in  $\mathcal{X}$  for which  $X_n \cap [\mathbf{x}, \mathbf{x} + \nu \mathbf{1}] = \emptyset$ . Define the constants  $\gamma_d$  using the induction  $\gamma_d := 2d(1 + \gamma_{d-1})$  with base case  $\gamma_1 := 2$ . Our first main result, whose proof is contained in Appendix B.4, concerns the finite-smoothness case where polynomial-order acceleration can be achieved:

**Theorem 2** (Higher-order convergence; finite smoothness). *Let  $\mathcal{X} = [\mathbf{0}, \mathbf{1}] \subset \mathbb{R}^d$  and  $X_n \subset \mathcal{X}$ . Let  $\mathcal{X}_h = [\mathbf{0}, h\mathbf{1}]$  and  $X_n^h = \{h\mathbf{x} : \mathbf{x} \in X_n\}$  where  $h \in (0, 1]$ . Assume that  $f \in \mathcal{H}_k(\mathcal{X})$ ,  $b \in \pi_r(\mathcal{X})$  and  $k_e \in C^{2s}(\mathcal{X} \times \mathcal{X})$ . Let  $m_n^h[f](\mathbf{0})$  denote the point estimate (6) based on data  $f(X_n^h)$ . Then there is an explicit  $n$ - and  $h$ -independent constant  $C_{r,s}$ , defined in the proof, such that*

$$\underbrace{|f(\mathbf{0}) - m_n^h[f](\mathbf{0})|}_{\text{extrapolation error}} \leq C_{r,s} \rho_{X_n, \mathcal{X}}^s |f|_{\mathcal{H}_k(\mathcal{X})} \underbrace{h^s}_{\text{acceleration}} \underbrace{\|b\|_{L^\infty(\mathcal{X}_h)}}_{\text{original bound}}$$

whenever the box fill distance satisfies  $\rho_{X_n, \mathcal{X}} \leq 1/(\gamma_d(r + 2s))$ .

To interpret the conclusion of Theorem 2, fix  $n$  to be large enough that the constraint on the box fill distance is satisfied and examine the convergence of  $m_n^h[f](\mathbf{0})$  to  $f(\mathbf{0})$  as  $h$  is decreased. If the problem possesses no additional smoothness to exploit (i.e.,  $s = 0$ ) then convergence is gated at the rate  $\|b\|_{L^\infty(\mathcal{X}_h)}$  of the original numerical method, irrespective of the number  $n$  of data that are used to train the GP. On the other hand, if  $f$  is regular enough that the normalised error functional  $\mathbf{x} \mapsto (f(\mathbf{x}) - f(\mathbf{0}))/b(\mathbf{x})$  is an element of the RKHS  $\mathcal{H}_{k_e}(\mathcal{X})$  of an  $s$ -smooth kernel (implied by  $|f|_{\mathcal{H}_k(\mathcal{X})} < \infty$ ), then the  $h^s$  factor provides acceleration of polynomial order  $s$  over the convergence rate of the original numerical method. To the best of our knowledge these theoretical results are the first of their kind for convergence

acceleration using GPs. Examples 5 and 8 illustrate cases in which our regularity assumptions are satisfied. For the reader’s convenience, we recall some standard examples of kernels and their associated smoothness properties in Appendix A.

**Remark 3** (Sample efficiency compared to Richardson). *A notable feature of Richardson extrapolation is that, under appropriate regularity assumptions, acceleration of order  $s$  can be achieved using a dataset of size  $n = s + 1$  in dimension  $d = 1$ . For example, if  $f$  is first-order accurate with  $f(h) = f(0) + c_1h + O(h^2)$ , then the line that passes through data  $(h, f(h))$  and  $(2h, f(2h))$  has intercept  $2f(h) - f(2h)$ , which is equal to  $2[f(0) + c_1h + O(h^2)] - [f(0) + 2c_1h + O(h^2)] = f(0) + O(h^2)$ ; an additional order of accuracy is gained. Our result is less sample-efficient, in the sense that  $n \geq 2r + 4s$  data are in principle required, due to the constraint on the box fill distance in Theorem 2. However, we speculate that this lower bound on  $n$  is not tight, and we empirically confirm that order- $s$  acceleration is observed at smaller sample sizes  $n$  in Examples 5 and 8.*

On the other hand, if there is infinite smoothness to exploit, then we may consider increasing the value of  $s$  in Theorem 2 to obtain an arbitrarily fast convergence rate as  $h \rightarrow 0$ , albeit with an increasing number  $n$  of training points required for the bound to hold. This result goes beyond classical Richardson extrapolation, but is natural within the GP framework. Theorem 4, whose proof is contained in Appendix B.5, is obtained by carefully tracking the  $s$ -dependent constants appearing in Theorem 2:

**Theorem 4** (Higher-order convergence; infinite smoothness). *In the setting of Theorem 2, assume further that  $k_e \in C^\infty(\mathcal{X} \times \mathcal{X})$  and that  $\sup_{\mathbf{x}, \mathbf{y} \in \mathcal{X}} \sum_{|\beta|=2s} |\partial_{\mathbf{y}}^\beta k_e(\mathbf{x}, \mathbf{y})| \leq C_k^{2s}(2s)!$  for some constant  $C_k$ . Then there exists an explicit  $h$ -independent constant  $C_{n,r,s}$ , defined in the proof, such that*

$$\underbrace{|f(\mathbf{0}) - m_n^h[f](\mathbf{0})|}_{\text{extrapolation error}} \leq C_{n,r,s} |f|_{\mathcal{H}(k)} \underbrace{h^{\frac{1}{4\gamma_d \rho_{X_n, \mathcal{X}}}}}_{\text{acceleration}} \underbrace{\|b\|_{L^\infty(\mathcal{X}_h)}}_{\text{original bound}}$$

whenever the box fill distance satisfies  $\rho_{X_n, \mathcal{X}} \leq \min\{1/(2\gamma_d(r+1)), 1/(2d^{1/2}\gamma_d e^{4d\gamma_d+1})\}$ .

The derivative growth condition in the statement of Theorem 4 holds for most popular smooth kernels  $k_e$ , including the Gaussian kernel. The order of acceleration is now determined by the box fill distance, which reflects the general phenomenon that “more samples are required to exploit smoothness” (Cabannes and Vigogna, 2023).

To assess the sharpness of our results we first consider the problem of approximating derivatives using finite differences; a setting where extrapolation methods are routinely used (see Section 6.7 of Brezinski and Zaglia, 2013):

**Example 5** (Higher-order convergence for finite difference approximation). *Consider numerical differentiation of a suitably regular function  $\psi : \mathbb{R} \rightarrow \mathbb{R}$ . The central difference method*

$$f(x) := \frac{\psi(t+x) - \psi(t-x)}{2x}, \quad x > 0,$$

is a second-order approximation to  $\psi'(t)$  for a given  $t \in \mathbb{R}$ . To make use of our results we set  $b(x) = x^2$ , from (3), and suppose that  $\psi(t+x) = c_0 + c_1x + c_2x^2 + c_3(x)x^3$  for some  $c_0, c_1, c_2 \in \mathbb{R}$  and some  $x$ -dependent coefficient  $c_3(x)$ . The normalised error is

$$e(x) = \frac{f(x) - f(0)}{b(x)} = \frac{\psi(t+x) - \psi(t-x)}{2x \cdot x^2} - \frac{\psi'(t)}{x^2} = \frac{c_3(x) - c_3(-x)}{2},$$

so that the assumptions of Theorem 2 are satisfied when  $x \mapsto c_3(x)$  and  $x \mapsto c_3(-x)$  are elements of  $\mathcal{H}_{k_e}(\mathcal{X})$ , and  $k_e \in C^{2s}(\mathcal{X} \times \mathcal{X})$  (the latter condition can be satisfied for example by taking  $k_e$  to be either a Matérn kernel or a Wendland kernel with appropriate smoothness level; see Appendix A). As a test problem, consider  $\psi(t) = \sin(10t) + 1_{t>0}t^{s+4}$ , with  $\psi'(0) = 10$  the value to be estimated; in Appendix B.6 we verify that our assumption on the form of  $\psi$  is satisfied. The sample size  $n = 5$  was fixed and the initial design  $X_n = \{0.2, 0.4, 0.6, 0.8, 1\}$  was scaled by a factor  $h$  to obtain a range of designs  $X_n^h \subset (\mathbf{0}, h\mathbf{1}]$ . In these experiments we work in 100 digits of numerical precision, so that rounding error can be neglected.

Results for  $s = 2$  are reported in Figure 2, with the absolute error  $|f(0) - m_n^h[f](0)|$  plotted as a function of  $h$  in the left panel. These results reveal that the orders of acceleration predicted by our analysis are achieved, despite the sample size  $n$  being less than that required to fulfill the box fill distance requirement in Theorem 2. The GRE method demonstrated accuracy comparable to Richardson's extrapolation method (and superior to other classical extrapolation methods) when the kernel was chosen to match the smoothness of the task at hand. Interestingly, the most accurate extrapolation was provided by GRE with the Gaussian kernel, despite this kernel being too smooth for the task at hand. The coverage of GRE credible intervals was also investigated, with the relative error  $(f(0) - m_n^h[f](0))/\sqrt{k_n[f](0,0)}$  plotted as a function of  $h$  in the right panel. It was found that credible intervals are asymptotically conservative in the case where a kernel with finite smoothness was used, in the sense that the relative error appeared to vanish in the  $h \rightarrow 0$  limit. However, in the case of the Gaussian kernel the credible intervals appeared to be asymptotically calibrated, in the sense that the relative error appeared to converge to a finite value ( $\approx 3$ ) in the  $h \rightarrow 0$  limit. Theoretical analysis of the GRE credible intervals is provided in Section 2.6.

Though they accurately describe the convergence acceleration provided by the GRE method, there are at least two apparent drawbacks with Theorems 2 and 4. The first is that these results require the error bound  $b$  to be a polynomial; this is an intrinsic part of our proof strategy, which is based on local polynomial reproduction, and cannot easily be relaxed. However, for applications in which a non-polynomial error bound  $\tilde{b}$  naturally arises, we may still be able to construct a polynomial error bound  $b \in \pi_r(\mathcal{X})$  for some  $r$  that satisfies  $\tilde{b}(\mathbf{x}) \leq b(\mathbf{x})$  for all  $\mathbf{x} \in \mathcal{X}$  and enables the conclusion of Theorem 2 to be applied. The second limitation is that, for many iterative numerical methods that produce a convergent sequence of approximations to the continuum quantity  $f(\mathbf{0})$  of interest, there is not always the notion of a continuum of discretisation parameters  $\mathbf{x}$  that can be exploited in the GRE framework. This second issue can be elegantly addressed using the notion of an  $s$ -smooth extension, which we introduce next.

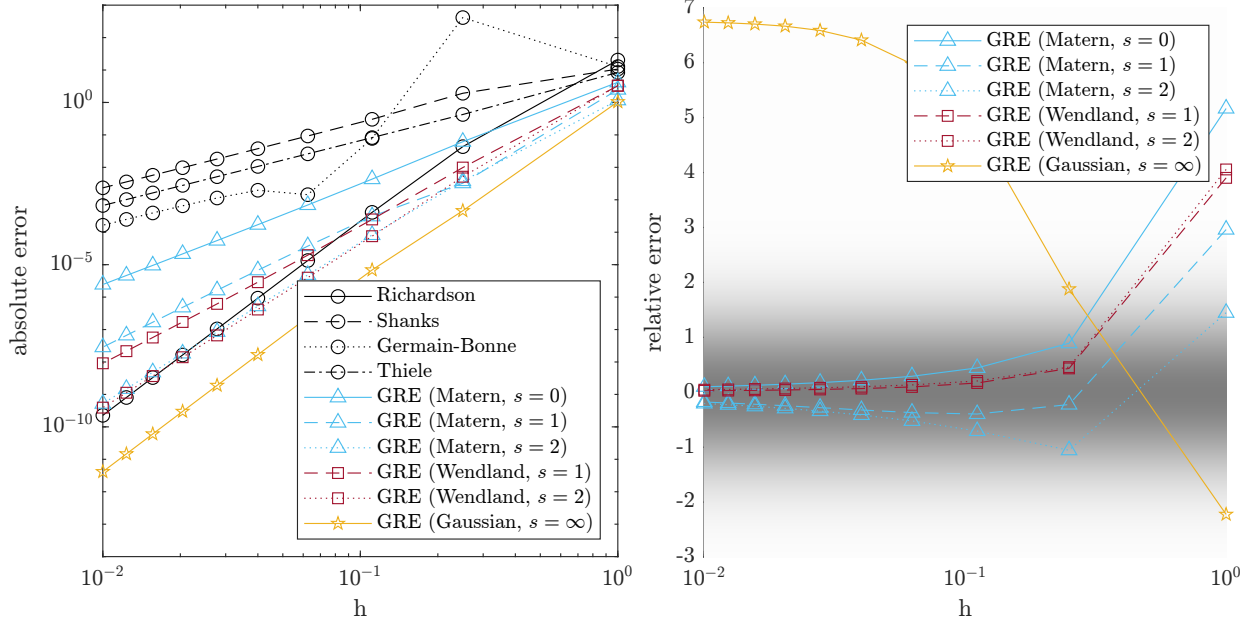


Figure 2: Accelerating the central difference method; Example 5. The left panel presents the absolute error  $|f(0) - m_n^h[f](0)|$ , while the right panel presents the relative error  $(f(0) - m_n^h[f](0))/\sqrt{k_n[f](0,0)}$ . Classical extrapolations methods (black circles) were compared to our Gauss–Richardson Extrapolation (GRE) method, with either a Matérn (blue triangles), Wendland (red squares), or Gaussian (yellow stars) kernel. The true smoothness in this case is  $s = 2$ , while the legend indicates the level of smoothness assumed by the kernel. Kernel length-scale parameters were set to  $\ell = 1$  and the scale estimator  $\sigma_n^2[f]$  proposed in Section 2.6 was used. Shaded regions in the right panel correspond to the density function of the standard normal.

## 2.5 The Generality of Continua

Several numerical methods do not admit a continuum of discretisation parameters  $\mathbf{x}$  that can be exploited in the GRE method. For example, the conjugate gradient algorithm for approximating the solution to a linear system of equations produces a convergent sequence of approximations, but is in no sense continuously indexed. The aim of this section is to demonstrate that iterative methods, which produce a sequence of approximations converging to a limiting quantity of interest, do in fact fall within our framework. The idea, roughly speaking, is to construct a function  $f$  whose values  $f(x_n)$  on a convergent sequence, such as  $x_n = 1/n$ , coincide with the approximation produced after  $n$  iterations of the numerical method. The challenge is to show that such a function  $f$  exists with sufficient regularity that the results of Section 2.4 can be applied. Our main tool is the idea of a  $p$ -smooth extension, which is the content of Proposition 6. Let  $\min(\mathbf{z}) := \min\{z_1, \dots, z_d\}$  for  $\mathbf{z} \in \mathbb{R}^d$ .

**Proposition 6** ( $p$ -smooth extension). *Suppose that  $C^p(\mathcal{X}) \subset \mathcal{H}_{k_e}(\mathcal{X})$  for some  $p \in \mathbb{N}$ . Let  $(\mathbf{x}_n)_{n \in \mathbb{N}} \subset \mathcal{X} \setminus \{\mathbf{0}\}$  be such that  $\mathbf{x}_{n+1} < \mathbf{x}_n$  componentwise and  $\mathbf{x}_n \rightarrow \mathbf{0}$ . Let  $(y_n)_{n \in \mathbb{N}}$  be a convergent sequence with limit  $y_\infty$ , such that the normalised errors  $e_n := (y_n - y_\infty)/b(\mathbf{x}_n)$*

satisfy  $|e_n - e_{n+1}| / \min(\mathbf{x}_n - \mathbf{x}_{n+1})^p \rightarrow 0$ . Then there exists a function  $f$  such that  $f(\mathbf{0}) = y_\infty$ ,  $f(\mathbf{x}_n) = y_n$  for each  $n \in \mathbb{N}$ , and  $|f|_{\mathcal{H}_k(\mathcal{X})} < \infty$ .

A polynomial expansion can be used to establish the preconditions of Proposition 6, as we illustrate in the following result:

**Corollary 7** (Sufficient conditions for  $p$ -smooth extension in  $d = 1$ ). *Let  $(x_n, y_n)_{n \in \mathbb{N}} \subset (0, \infty) \times \mathbb{R}$  be such that  $x_n$  converges monotonically to 0, with  $(x_n^{p+1} - x_{n+1}^{p+1})(x_n - x_{n+1})^{-p} \rightarrow 0$ ,  $x_n^{p+2}(x_n - x_{n-1})^{-p} \rightarrow 0$  and  $y_n = y_\infty + C_1 x_n^r + C_2 x_n^{r+p+1} + O(x_n^{r+p+2})$  for some constants  $y_\infty, C_1, C_2 \in \mathbb{R}$ . Let  $b(x) = x^r$ . Then the preconditions of Proposition 6 are satisfied.*

The proof of both Proposition 6 and Corollary 7 can be found in Appendix B.7. The conditions on the sequence  $(x_n)_{n \in \mathbb{N}}$  in Corollary 7 are satisfied by, for example, sequences of the form  $x_n = \frac{1}{n}$  and  $x_n = \lambda^{-n}$  for any  $\lambda > 1$ , which are the sort of expressions that routinely appear in error bounds. The overall approach is illustrated in Example 8, where a GP analogue of the classical Romberg method for numerical integration is derived.

**Example 8** (GP Romberg methods). *Romberg methods for numerical integration are classically obtained via Richardson extrapolation of the trapezoidal rule (Brezinski and Zaglia, 2013, Section 6.7); it is interesting to ask if a similar feat can be achieved with GRE. Let  $\psi \in C^{2m+2}([0, 1])$  and consider the trapezoidal rule  $y_n := \frac{1}{n}[\frac{\psi(0)}{2} + \psi(\frac{1}{n}) + \dots + \psi(\frac{n-1}{n}) + \frac{\psi(1)}{2}]$ . The Euler–Maclaurin summation formula implies that the error of the trapezoidal rule can be expressed as*

$$y_n - \int_0^1 \psi(t) dt = \sum_{i=1}^m \frac{B_{2i}}{(2i)!} x_n^{2i} (\psi^{(2i-1)}(1) - \psi^{(2i-1)}(0)) + \frac{B_{2m+2}}{(2m+2)!} x_n^{2m+2} \psi^{(2m+2)}(\beta_n)$$

for some  $\beta_n \in [0, 1]$ , where  $x_n = \frac{1}{n}$  and  $B_k$  are the Bernoulli numbers. As a test problem, consider  $\psi(t) = \sin(10t) + t^2$ , for which we can apply Corollary 7 with  $b(x) = x^2$ ,  $r = 2$  and  $p = 3$ . Thus there exists a function  $f$  that agrees with the trapezoidal rule on  $(x_n)_{n \in \mathbb{N}}$  and satisfies the preconditions of Theorem 2 for a kernel  $k_e$  with smoothness up to  $s = 2$ ; see Appendix A. Empirical results in Figure 3 verify that we are indeed able to gain an additional  $s = 2$  convergence orders over the original trapezoidal rule, akin to Romberg integration, using our GRE method. Here the sample size  $n = 5$  was fixed and the initial design  $X_n = \{1, \frac{1}{2}, \frac{1}{4}, \frac{1}{8}, \frac{1}{16}\}$  was scaled by a factor  $h$  to obtain a range of designs  $X_n^h \subset (\mathbf{0}, h\mathbf{1}]$ . The accuracy of the GRE point estimator and the coverage of the GRE credible interval demonstrate similar behaviour to that observed in Example 5.

These results extend the applicability of GRE to settings where components of the discretisation parameter vector  $\mathbf{x}$  could take values in any infinite set. For example, in standard implementations of the finite element method for numerically solving partial differential equations one has a continuous parameter, characterising the width of a triangular mesh, a discrete parameter, characterising the number of cubature nodes used to integrate against each element, and another discrete parameter, specifying the number of iterations of a conjugate gradient method to solve the resulting linear system. The resulting mixture of continuous and discrete discretisation parameters  $\mathbf{x}$  falls within the scope of our GRE method.

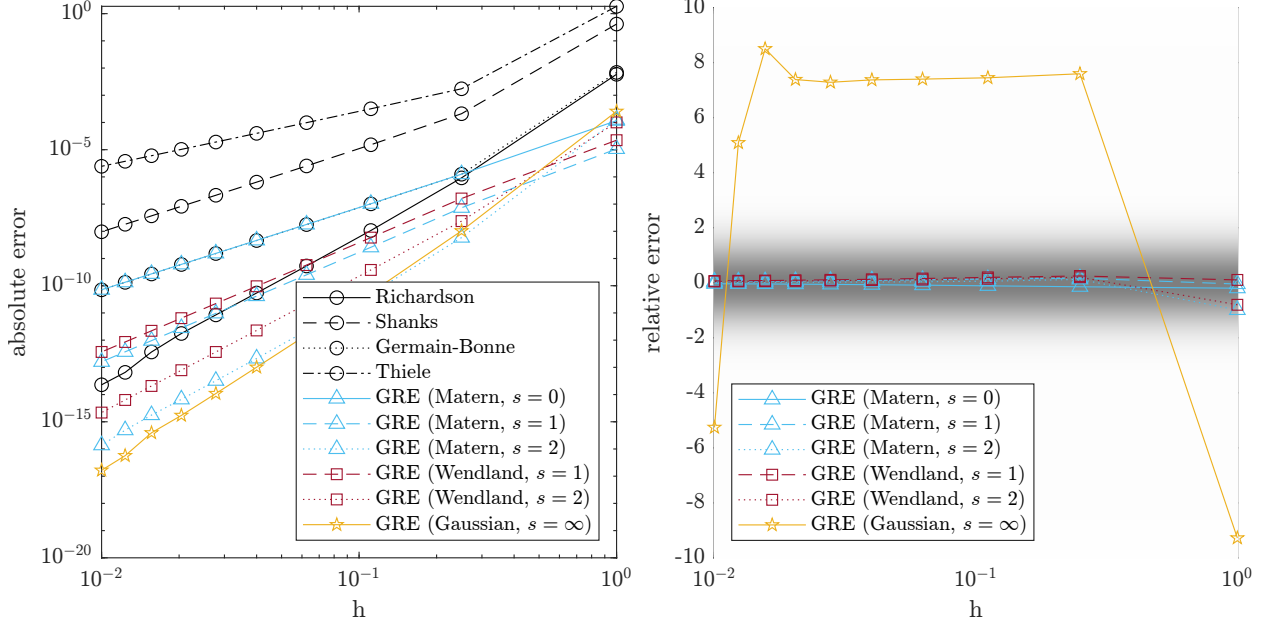


Figure 3: Accelerating the trapezoidal method to obtain a GP Romberg method; Example 8. The left panel presents the absolute error  $|f(0) - m_n^h[f](0)|$ , while the right panel presents the relative error  $(f(0) - m_n^h[f](0))/\sqrt{k_n[f](0,0)}$ . Classical extrapolations methods (black circles) were compared to our Gauss–Richardson Extrapolation (GRE) method, with either a Matérn (blue triangle), Wendland (red squares), or Gaussian (yellow stars) kernel. The true smoothness in this case is  $s = 2$ , while the legend indicates the level of smoothness assumed by the kernel. Kernel length-scale parameters were set to  $\ell = 1$ . Shaded regions in the right panel correspond to the density function of the standard normal.

## 2.6 Uncertainty Quantification

An encouraging observation from Examples 5 and 8 was that the GRE credible intervals were not asymptotically over-confident as  $h \rightarrow 0$ . The aim of this section is to explain how the scale parameter  $\sigma^2$  in (3), which controls the size of credible intervals  $C_\alpha[f]$  in (7), was actually estimated, and to rigorously prove that asymptotic over-confidence cannot occur when our proposed estimator  $\sigma_n^2[f]$  is used.

The most standard approach to kernel parameter estimation is maximum (marginal) likelihood, but in GRE we do not have a valid likelihood due to taking the improper  $k_0^2 \rightarrow \infty$  limit. Instead, we motivate a particular estimator  $\sigma_n^2[f]$  using asymptotic guarantees for the associated credible interval. Specifically, we advocate the estimator

$$\sigma_n^2[f] := \frac{|m_n[f]|_{\mathcal{H}_k(x)}^2}{n} = \frac{1}{n} \left[ f(X_n)^\top \mathbf{K}_b^{-1} f(X_n) - \frac{(\mathbf{1}^\top \mathbf{K}_b^{-1} f(X_n))^2}{\mathbf{1}^\top \mathbf{K}_b^{-1} \mathbf{1}} \right], \quad (8)$$

which takes the same form as the maximum likelihood estimator that we would have obtained had we not taken the  $k_0^2 \rightarrow \infty$  limit, but with the semi-norm  $|m_n[f]|_{\mathcal{H}_k(x)}$  in place of the

conventional norm on  $\mathcal{H}_k(\mathcal{X})$ . This choice is supported by the following asymptotic result, whose proof is contained in Appendix B.8:

**Proposition 9** (Asymptotic over-confidence is prevented). *In the setting of Theorem 2, suppose that  $s \geq 1$  and that  $\lim_{\mathbf{x} \rightarrow \mathbf{0}} b(\mathbf{x})^{-1}(f(\mathbf{x}) - f(\mathbf{0})) \neq 0$  (i.e. we have a sharp error bound). Let  $m_n^h[f](\mathbf{0})$  and  $k_n^h[f](\mathbf{0}, \mathbf{0})$  denote the conditional mean and variance in (6), based on data  $f(X_n^h)$  and the estimator in (8). Then*

$$\limsup_{h \rightarrow 0} \frac{|f(\mathbf{0}) - m_n^h[f](\mathbf{0})|}{\sqrt{k_n^h[f](\mathbf{0}, \mathbf{0})}} < \infty$$

whenever the box fill distance  $\rho_{X_n, \mathcal{X}}$  is sufficiently small.

In other words, the width  $\sqrt{k_n[f](\mathbf{0}, \mathbf{0})}$  of the credible interval cannot vanish asymptotically faster than the actual absolute error  $|f(\mathbf{0}) - m_n[f](\mathbf{0})|$ . Though this result does not guarantee that credible intervals are the ‘right size’ *per se*, there is no randomness in the data-generating process  $f(\mathbf{x})$  and thus standard statistical notions of coverage, or ‘right size’, cannot be directly applied (see Karvonen et al., 2020). In practice, we have already seen empirical evidence that the credible sets (7) are appropriately conservative; an arguably predictable consequence of the conservative GP prior discussed in Section 2.3. Note that the conclusion of Proposition 9 also holds when the stronger hypotheses of Theorem 4 are assumed. However, the result assumes that a kernel with appropriate smoothness is used; it does not explain the behaviour of GRE with the Gaussian kernel observed in Examples 5 and 8, since in that case the Gaussian kernel was formally misspecified.

Assured that our credible intervals are in a sense meaningfully related to the actual error, we can now proceed to exploit this measure of uncertainty for experimental design.

## 2.7 Optimal Experimental Design

One of the main engineering challenges associated with the simulation of continuum mathematical or physical phenomena is the numerical challenge of simultaneously controlling all sources of discretisation error, to ensure the output  $f(\mathbf{x})$  remains close in some sense to  $f(\mathbf{0})$ , the continuum quantity of interest. In practice, one might explore the sensitivity of the simulator output  $f(\mathbf{x})$  to small changes in each discretisation parameter  $x_i$  in turn, to heuristically identify a global setting  $\mathbf{x}_{\text{hi-fi}}$  which is then fixed for the lifetime in which the simulator is used. It seems remarkable that more principled methodology has not yet been developed, and we aim to fill this gap by formulating *optimal experimental design* within the GRE framework.

The accuracy of the point estimator (6) will depend crucially on the locations at which the GP has been trained. Section 2.6 established that the conditional variance is meaningfully related to estimation accuracy, with the advantage that it can be explicitly calculated. This motivates the following cost-constrained optimisation problem

$$\arg \max_{X \subset \mathcal{D}} \mathbf{1}^\top \mathbf{K}_b^{-1} \mathbf{1} \quad \text{s.t.} \quad \sum_{\mathbf{x} \in X} c(\mathbf{x}) \leq C, \quad (9)$$



where  $\mathcal{D} \subseteq \mathcal{X}$  denotes the set of feasible simulations being considered,  $\mathbf{K}_b$  is the matrix with entries  $k_b(\mathbf{x}_i, \mathbf{x}_j)$ ,  $\mathbf{x}_i, \mathbf{x}_j \in X$ , the map  $c : \mathcal{D} \rightarrow \mathbb{R}$  quantifies the cost associated with obtaining simulator output  $f(\mathbf{x})$ , and  $C$  denotes the total computational budget. This numerical analysis-informed objective  $\mathbf{1}^\top \mathbf{K}_b^{-1} \mathbf{1}$  is inversely proportional to the GRE posterior variance (6) when the scale parameter  $\sigma$  is fixed, rather than estimated (since *a priori* we do not suppose data have been obtained from which  $\sigma$  could be estimated). This optimisation does not enforce a particular training sample size  $n$ , it just constrains the total computational cost. As such, (9) represents a challenging optimisation problem, with both the number  $n$  of experiments in the optimal design, and the optimal experiments  $X = \{\mathbf{x}_i\}_{i=1}^n$  themselves, to be determined. To proceed, we consider a finite set  $\mathcal{D}$  of candidate experiments and then use brute force to search for an optimal design restricted to this candidate set.

**Example 10** (Optimal experimental design in  $d = 1$ ). *Consider a first-order numerical method with linear cost, so that  $b(x) = x$  and  $c(x) = x^{-1}$ , an example of which would be the classical forward Euler method. For illustration we take  $k_e$  to be either a Matérn kernel ( $s = 0$ ) or the Gaussian kernel ( $s = \infty$ ), in each case with length-scale  $\ell = 1$  fixed. The total computational budget  $C$  was varied and optimal designs  $X$  were computed with elements constrained to a size 20 grid  $\mathcal{D}$ ; results are shown in Figure 4. In the case of a rough kernel, like the Matérn kernel, a greedy/exploitative strategy of assigning all compute power to the highest resolution experiment seems optimal. Since we are working only with a discrete set of experiments, there is a small residual computational budget that is allocated to one or two further cheap experiments. For the Gaussian kernel, the optimal strategy is less greedy, with optimal designs involving more experiments, indicating that the greater smoothness is being leveraged to improve the accuracy of GRE.*

In practice a small number of preliminary simulations should be used to estimate appropriate length-scale parameters  $\ell$  for the covariance kernel. Such parameter estimation becomes more critical in the multivariate setting, illustrated in the right panel of Figure 4, since the simulator output  $f(\mathbf{x})$  may be more or less sensitive to different components of  $\mathbf{x}$ ; in Section 3 a practical workflow is presented.

**Remark 11** (Trivial solution for iterative methods). *In Section 2.5 we discussed the scenario where data are generated along a sequence  $(\mathbf{x}_n)_{n \in \mathbb{N}}$  by an iterative method, which first produces  $f(\mathbf{x}_1), \dots, f(\mathbf{x}_{n-1})$  en route to producing the final output  $f(\mathbf{x}_n)$ . In this scenario the cost of computing  $f(\mathbf{x}_1), \dots, f(\mathbf{x}_n)$  is simply  $c(\mathbf{x}_n)$ , in which case computing as many iterations as possible is optimal in the sense of (9).*

The methodology just presented systematises the often *ad-hoc* process of selecting appropriate fidelities on which simulator output is computed, in a manner that is specifically tailored to improving the accuracy of our GRE method. Sequential experimental design strategies can also be developed, but were not pursued. The remainder of this section deals with three important generalisations of the GRE method; the case where convergence orders are unknown and must be estimated (Section 2.8), the case of multivariate simulator output (Section 2.9), and the case where the simulator contains additional degrees of freedom (Section 2.10).

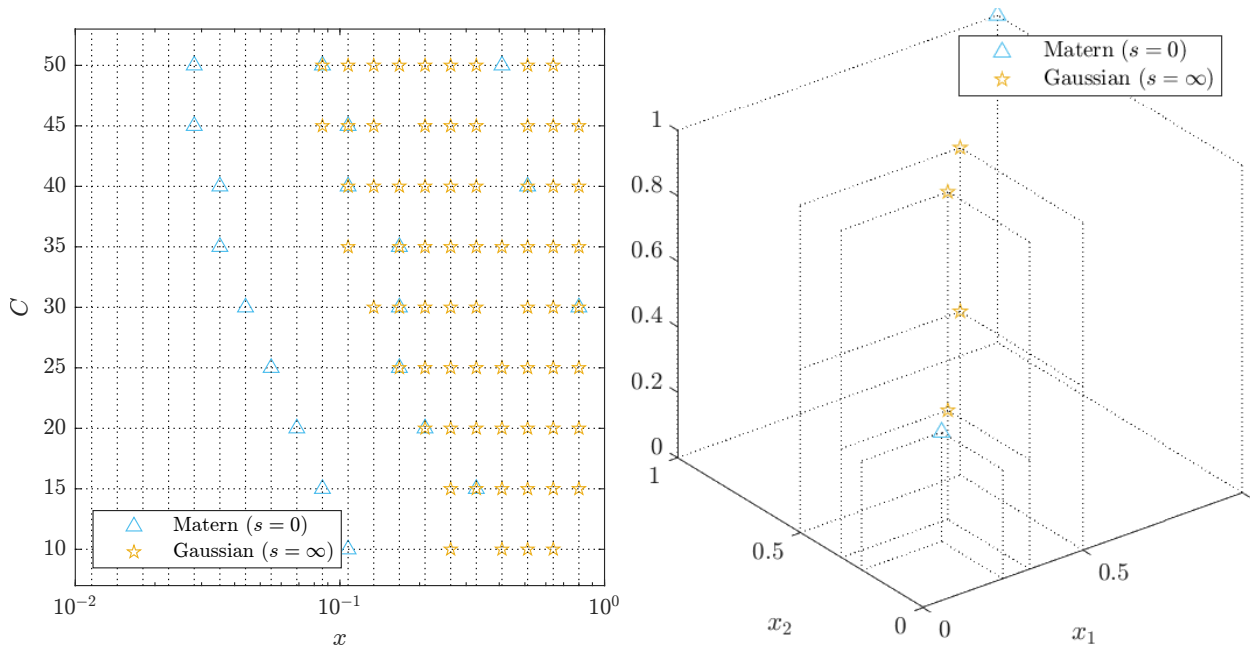


Figure 4: Optimal experimental designs were computed, for varying total computational budgets  $C$ , using either a Matérn (blue triangles;  $s = 0$ ) or Gaussian (yellow stars;  $s = \infty$ ) kernel. Left: The setting of Example 10, with candidate states shown as vertical dotted lines on the plot. Right: An illustration of experimental design in dimension  $d = 3$ , with dotted lines used to indicate the coordinates of the states that were selected.

## 2.8 Extension to Unknown Convergence Order

The practical application of extrapolation methods does not necessarily require access to an explicit error bound, as several procedures have been developed to automatically identify a suitable method from a collection of extrapolation methods (which could correspond to different assumed convergence orders, or different classes of extrapolation method). A representative approach, called *automatic selection* (Delahaye, 1981), is based on the idea that small changes  $S_{n+1} - S_n$  between consecutive iterates is a useful proxy for the convergence rate of an extrapolation method  $(S_n)_{n \in \mathbb{N}}$ . Another approach is to linearly combine estimates produced by a collection of extrapolation methods, called a *composite sequence approach* (Brezinski, 1985). From our statistical standpoint, these methods bear a respective semblance to model selection and model averaging. Pursuing a statistical perspective on extrapolation, here we consider maximum (marginal) likelihood as a default for selecting an appropriate GP prior model for GRE. The  $k_0^2 \rightarrow \infty$  limit taken in Section 2.2 means that we do not have a proper likelihood, so instead we identify and maximise an appropriate *quasi* likelihood. Our justification is twofold, namely (1) our quasi likelihood is directly analogous to the standard GP likelihood, and (2) we provide analysis below that demonstrates the consistency of maximum quasi likelihood for estimation of convergence order in the GRE framework.

To formulate the main result of this section, we suppose we have a vector  $\mathbf{r} \in \mathbb{R}^p$  that parametrises the error bound  $b_{\mathbf{r}} : \mathcal{X} \rightarrow [0, \infty)$ , with the interpretation that increasing the value of any of the components of  $\mathbf{r}$  corresponds to faster convergence of the error bound  $b_{\mathbf{r}}(\mathbf{x})$  to  $\mathbf{0}$  as  $\mathbf{x} \rightarrow \mathbf{0}$ . Specifically, we call a class of error bounds *monotonically parametrised* if, for all  $\mathbf{r}_1 < \mathbf{r}_2$  we have

$$\inf_{\mathbf{r} \leq \mathbf{r}_1} \lim_{\mathbf{x} \rightarrow \mathbf{0}} \frac{b_{\mathbf{r}_2}(\mathbf{x})}{b_{\mathbf{r}}(\mathbf{x})} = 0.$$

This is not a restriction *per se*, as we are free to choose how  $b_{\mathbf{r}}$  is parametrised, but an assumption of this kind is required to enable the following result to be rigorously stated. Examples of monotonically parametrised error bounds include  $b_{\mathbf{r}}(\mathbf{x}) = x_1^{r_1} + \dots + x_d^{r_d}$  and  $b_{\mathbf{r}}(\mathbf{x}) = x_1^{r_1} \dots x_d^{r_d}$ , which are the sort of expressions that routinely appear in error bounds. The proof of the following result can be found in Appendix B.9:

**Proposition 12** (Estimation using maximum quasi likelihood). *Let  $X_n^h = \{h\mathbf{x} : \mathbf{x} \in X_n\}$ . Suppose that  $f \in \mathcal{H}_k(\mathcal{X})$  holds when  $k$  in (3) is based on the monotonically parametrised bound  $b_{\mathbf{r}_0}(\mathbf{x})$  for some  $\mathbf{r}_0 \geq \mathbf{0}$ . Let  $\mathbf{K}_{b_{\mathbf{r}},h}$  denote the matrix with entries  $k_{b_{\mathbf{r}}}(h\mathbf{x}_i, h\mathbf{x}_j)$ , where the dependence of this matrix on both  $h$  and  $\mathbf{r}$  has now been emphasised, relative to the notation  $\mathbf{K}_b$  introduced in Section 2.2. Then any maximiser  $\mathbf{r}_n^h[f] \in \arg \max_{\mathbf{r} \geq \mathbf{0}} \mathcal{L}_n^h(\mathbf{r})$  of the log-quasi (marginal) likelihood*

$$\mathcal{L}_n^h(\mathbf{r}) := -f(X_n^h)^\top \mathbf{K}_{b_{\mathbf{r}},h}^{-1} f(X_n^h) + \frac{(\mathbf{1}^\top \mathbf{K}_{b_{\mathbf{r}},h}^{-1} f(X_n^h))^2}{\mathbf{1}^\top \mathbf{K}_{b_{\mathbf{r}},h}^{-1} \mathbf{1}} - \log \det \mathbf{K}_{b_{\mathbf{r}},h} \quad (10)$$

satisfies  $\liminf_{h \rightarrow 0} \mathbf{r}_n^h[f] \geq \mathbf{r}_0$ .

The first two terms in (10) correspond to the (square of the) semi-norm  $|m_n^h[f]|_{\mathcal{H}_k(X)}$ , which is the analogue of the usual  $\|m_n^h[h]\|_{\mathcal{H}_k(X)}$  term that we would appear in the likelihood had we not taken the  $k_0^2 \rightarrow \infty$  limit; this justifies the interpretation of (10), up to constants, as a quasi-likelihood. The one-sided conclusion of Proposition 12 may be surprising at first, but this is in fact the strongest result that can be expected. Indeed, the statement that  $f(\mathbf{x}) - f(\mathbf{0}) = O(b_{\mathbf{r}_0}(\mathbf{x}))$  does not rule out the possibility that the error  $f(\mathbf{x}) - f(\mathbf{0})$  decays *faster* than  $b_{\mathbf{r}_0}(\mathbf{x})$ , and in this case we would expect the estimator  $\mathbf{r}_n^h[f]$  to adapt to the actual convergence order. The experiments that we report in Section 3 used maximum quasi (marginal) likelihood whenever convergence orders and/or kernel length-scale parameters were estimated.

## 2.9 Generalisation to Multidimensional Output

Until this point we have considered the continuum quantity of interest  $f(\mathbf{0})$  to be scalar-valued. Oftentimes, however, we are interested in quantities  $\{f(\mathbf{0}, \mathbf{t})\}_{\mathbf{t} \in \mathcal{T}}$  that are vector- or function-valued depending on the nature of the index set  $\mathcal{T}$ . The E-algorithm that we described in Section 1 has been extended to finite-dimensional vector-valued output; see Chapter 4 of Brezinski and Zaglia (2013) for detail. A possible advantage of the GP-based

approach taken in GRE is that it does not impose any mathematical structure on  $\mathcal{T}$  beyond this being a set, making extension of the methodology to function-valued output straightforward.

To extend our methodology to multivariate output, let  $f : \mathcal{X} \times \mathcal{T} \rightarrow \mathbb{R}$  be such that  $\{f(\mathbf{0}, \mathbf{t})\}_{\mathbf{t} \in \mathcal{T}}$  is the continuum quantity of interest and  $f(\mathbf{x}, \mathbf{t})$  is a numerical approximation to  $f(\mathbf{0}, \mathbf{t})$ . For example,  $f(0, t)$  may represent the solution to an ordinary differential equation at time  $t$ , while  $f(x, t)$  may represent an approximation to this solution obtained using a Runge–Kutta method, with  $x$  being the error tolerance of the Runge–Kutta method. To improve presentation we will assume that  $f(\mathbf{x}, \mathbf{t}) - f(\mathbf{0}, \mathbf{t}) = O(b(\mathbf{x}))$  *uniformly* over  $\mathbf{t} \in \mathcal{T}$ , but  $\mathbf{t}$ -dependent error bounds could also be considered with additional notational overhead. Our original covariance function (3) can be generalised to

$$k((\mathbf{x}, \mathbf{t}), (\mathbf{x}', \mathbf{t}')) = \sigma^2 [k_0^2 + b(\mathbf{x})b(\mathbf{x}')k_e(\mathbf{x}, \mathbf{x}')] k_{\mathcal{T}}(\mathbf{t}, \mathbf{t}'), \quad \mathbf{x}, \mathbf{x}' \in \mathcal{X}, \mathbf{t}, \mathbf{t}' \in \mathcal{T}, \quad (11)$$

where, to exploit tractable computation that results from this tensor product kernel, we have assumed a tensor product kernel and will assume that data  $X_n = \{(\mathbf{x}_i, \mathbf{t}_j)\}_{i=1}^{n_1} \{j=1}^{n_2}$  are obtained on a Cartesian grid ( $n = n_1 n_2$ ). That is, with the data appropriately ordered we have the Kronecker decomposition  $\mathbf{K} = \mathbf{K}_{\mathcal{X}} \otimes \mathbf{K}_{\mathcal{T}}$ , where  $\mathbf{K}_{\mathcal{X}}$  is the matrix with entries  $k_0^2 + b(\mathbf{x}_i)b(\mathbf{x}_j)k_e(\mathbf{x}_i, \mathbf{x}_j)$ , and  $\mathbf{K}_{\mathcal{T}}$  is the matrix with entries  $k_{\mathcal{T}}(\mathbf{t}_i, \mathbf{t}_j)$ . Then analogous calculations to those detailed in Appendix B.2, which we present in Appendix B.10, show that for values of  $\mathbf{t}, \mathbf{t}'$  contained in the dataset, the conditional mean and covariance function in the  $k_0 \rightarrow \infty$  limit are

$$m_n[f](\mathbf{x}, \mathbf{t}) = \left\{ \mathbf{k}_b(\mathbf{x})^\top \mathbf{K}_b^{-1} + [1 - \mathbf{k}_b(\mathbf{x})^\top \mathbf{K}_b^{-1} \mathbf{1}] \frac{\mathbf{1}^\top \mathbf{K}_b^{-1}}{\mathbf{1}^\top \mathbf{K}_b^{-1} \mathbf{1}} \right\} \otimes [k_{\mathcal{T}}(\mathbf{t}) \mathbf{K}_{\mathcal{T}}^{-1}] f(X_n)$$

$$k_n[f](\mathbf{x}, \mathbf{t}), (\mathbf{x}', \mathbf{t}')) = \sigma_n^2[f] \left\{ k_b(\mathbf{x}, \mathbf{x}') k_{\mathcal{T}}(\mathbf{t}, \mathbf{t}') - [\mathbf{k}_{\mathcal{T}}(\mathbf{t})^\top \mathbf{K}_{\mathcal{T}}^{-1} \mathbf{k}_{\mathcal{T}}(\mathbf{t}')] \times \right.$$

$$\left. \left[ \mathbf{k}_b(\mathbf{x})^\top \mathbf{K}_b^{-1} \mathbf{k}_b(\mathbf{x}') - \frac{[\mathbf{k}_b(\mathbf{x})^\top \mathbf{K}_b^{-1} \mathbf{1} - 1][\mathbf{k}_b(\mathbf{x}')^\top \mathbf{K}_b^{-1} \mathbf{1} - 1]^\top}{\mathbf{1}^\top \mathbf{K}_b^{-1} \mathbf{1}} \right] \right\},$$

where  $\mathbf{k}_{\mathcal{T}}(\mathbf{t})$  is the vector with entries  $k_{\mathcal{T}}(\mathbf{t}_i, \mathbf{t})$ . For values of  $\mathbf{t}, \mathbf{t}'$  not contained in the training dataset, the conditional covariance does not have a finite limit; a proper prior should be used if off-grid prediction in the  $\mathbf{t}$ -domain is required. Further details on the multivariate setting are deferred to Section 3, where the approach is explored in the context of predicting temporal output from a cardiac model.

## 2.10 Incorporating Additional Degrees of Freedom

The final methodological extension that we consider is the case where  $f_{\boldsymbol{\theta}}(\mathbf{x})$  additionally depends on one or more degrees of freedom  $\boldsymbol{\theta} \in \Theta$ ; a setting where emulation or MFM methods are routinely used (c.f. Section 1). The proposed GRE method can be applied in this context by viewing  $f_{\boldsymbol{\theta}}(\mathbf{0})$  as a simulator with multidimensional output  $\{f(\mathbf{0}, \boldsymbol{\theta})\}_{\boldsymbol{\theta} \in \Theta}$  and then applying the methodology described in Section 2.9 with  $\boldsymbol{\theta}$ , rather than  $\mathbf{t}$ , indexing the

output of this extended model. Since the required calculations are identical, we do not dwell any further on this point.

This completes our exposition of the GRE method. Next we next turn to a cardiac modelling case study, where the usefulness of the methodology is evaluated.

### 3 Case Study: Cardiac Modelling

The cardiac model  $f_{\theta}(\mathbf{x})$  that we consider in this section is a detailed numerical simulation of a single heart beat<sup>1</sup> (Strocchi et al., 2023). The simulation is rooted in finite element methods that require both a spatial ( $x_1$ ) and a temporal ( $x_2$ ) discretisation level to be specified; of these, the spatial discretisation is the most critical, due to the  $O(x_1^{-3})$  cost associated with the construction of a suitable triangulation of the time-varying 3-dimensional volume of the heart; see Figure 5. The computational cost  $c(\mathbf{x})$  is measured in real computational time (seconds) and comprises the *setup time*, *assembly time* (the time taken to assemble linear systems of equations), and the *solver time* (the time taken to solve linear systems of equations), with assembly time the main contributor to total computational cost. To achieve a clinically-acceptable level of accuracy, it is typical for a simulation  $f_{\theta}(\mathbf{x}_{\text{default}})$  to be performed with  $\mathbf{x}_{\text{default}} \approx (0.4 \text{ mm}, 2 \text{ ms})$ , at a cost  $c(\mathbf{x}_{\text{default}}) \approx 1.5 \times 10^4$  seconds (around  $\approx 4$  hours) for a single heart beat<sup>2</sup>. This poses severe challenges to the scientific use of such models, with super-computing resources required to ascertain whether there are values of scientific parameters  $\theta$  for which observed data are consistent with model output (Strocchi et al., 2023). These challenges directly motivated the development of GRE, and the remainder of this paper is dedicated to exploring the value of extrapolation methods in this context. Extrapolation of the cardiac model output represents a much greater challenge compared to extrapolation for the examples considered in Section 2, due to the nonlinear physics being simulated. Since our focus in this paper is not on inference for  $\theta$ , these degrees of freedom were fixed to physically-realistic values based on previous analyses (Strocchi et al., 2020, 2023), with all further details on the construction of the cardiac model reserved for Appendix C.

Section 3.1 sets out a practical workflow for using the GRE method, that focuses on the multidimensional setting where both convergence orders and kernel length-scale parameters are to be estimated. The performance of GRE is then investigated for both scalar-valued (Section 3.2) and multivariate (Section 3.3) continuum quantities of interest.

---

<sup>1</sup>The simulation is usually run until a steady-state is reached before reading off quantities of interest, at a substantial increase to the overall computational cost. For the present purpose we removed components from the model that required multiple heart beats to reach a steady state, and simulated only a single heart beat.

<sup>2</sup>Simulations for this case study were performed on ARCHER2, a UK national super computing service (<https://www.archer2.ac.uk/>). Each simulation involved 512 CPUs operating in parallel, so that simulation of one heart beat using setting  $\mathbf{x}_{\text{default}}$  required  $\approx 4 \times 512$  CPU hours in total.

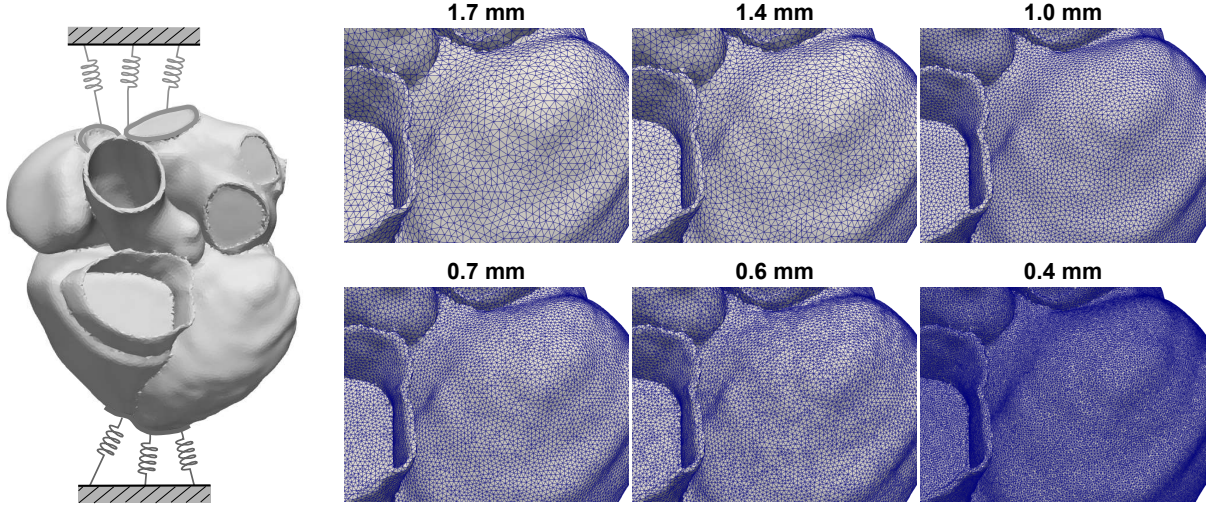


Figure 5: Cardiac model: Left: Schematic indicating the veins and the apical region where spring boundary conditions were applied. Right: A subset of the mesh resolutions used in this case study. The finest resolution required  $3 \times 10^7$  finite elements to be used.

### 3.1 A Proposed General Workflow

The sophistication of the cardiac model renders analytical derivation of convergence orders essentially impossible, so to proceed these orders must be estimated. However, the computational cost of simulating from the model means that data from which convergence orders can be estimated are necessarily limited. This motivates us to propose the following pragmatic workflow, which we present for a general model  $f(\mathbf{x})$  and which scales in a reasonable way with the number  $d$  of components of  $\mathbf{x}$  that can be varied. This workflow requires the user to specify a lo-fi setting  $\mathbf{x}_{\text{lo-fi}}$  as a starting point, together with a means to predict the computational cost  $c(\mathbf{x})$  of simulating  $f(\mathbf{x})$ , and a total computational budget  $C$ :

1. For each fidelity parameter  $x_i$ ,  $i = 1, \dots, d$ :
  - (a) Simulate  $f(\mathbf{x})$  for a range of values of  $x_i$ , with all of the other components  $\mathbf{x}$  held fixed to their values in  $\mathbf{x}_{\text{lo-fi}}$ .
  - (b) Fit a univariate numerical analysis-informed GP model (4, 5) to these data, assuming an error bound of the form  $b(x_i) = x_i^{r_i}$ , where the scale estimate  $\hat{\sigma}_i$  from Section 2.6 is used, and where the convergence order  $r_i$ , the kernel smoothness  $s_i$ , and the kernel length-scale parameter  $\ell_i$  are simultaneously estimated using quasi maximum likelihood, as explained in Section 2.8.
2. Construct a tensor product covariance model  $k_e(\mathbf{x}, \mathbf{x}') = k_e(x_1, x'_1; \ell_1) \dots k_e(x_d, x'_d; \ell_d)$  and posit the overall error bound  $b(\mathbf{x}) = \hat{\sigma}_1 x_1^{r_1} + \dots + \hat{\sigma}_d x_d^{r_d}$ . Then perform experimental design as described in Section 2.7, with computational budget  $C$ . Denote the optimal design  $X_n$ .

3. Simulate  $f(\mathbf{x})$  for each  $\mathbf{x} \in X_n$  and return the GRE conditional mean (6) as the final approximation to  $f(\mathbf{0})$ .

Several remarks are in order: First, it is assumed that the Step 1 incurs negligible cost relative to the total computational budget; the precise interpretation of this assumption will necessarily be context-dependent. Second, the additive form for  $b(\mathbf{x})$  is appropriately conservative, in the sense that *all* components of  $\mathbf{x}$  must be small to control this bound. One could go further and compare the performance of GPs based on alternative form of  $b(\mathbf{x})$ , for example with interaction terms included, selecting among such models using maximum quasi likelihood, but for the present purposes the additive form of  $b(\mathbf{x})$  is preferred since it is compatible with the independent estimation of convergence orders  $r_i$  in Step 1. Third, the independent estimation of  $(r_i, s_i, \ell_i)$  for each  $i = 1, \dots, d$  can be performed using brute-force search over a 3-dimensional grid to maximise the quasi-likelihood, whereas simultaneous estimation of all kernel parameters would be both statistically and computationally difficult. The full workflow is demonstrated on our cardiac case study, next.

### 3.2 Approximation of Scalar Quantities of Interest

The first part of our case study concerned the approximation of physiologically-interpretable scalar-valued quantities of interest. These were; the minimum volume of the left and right ventricles and atria, the maximum volume during ventricular contraction for the left and right atria, and the time taken for the ventricles to contract in total capacity by one half; a total of 7 test problems for GRE.

Though the computational time  $c(\mathbf{x}_{\text{default}})$  is substantial, in this case study parallel computation resources can be exploited. The main computational constraint that we work under here is that we will only run experiments for which  $c(\mathbf{x}) \leq c(\mathbf{x}_{\text{default}})$  within our GRE method. Since the continuum limit  $f(\mathbf{0})$  is intractable, we additionally computed a reference solution  $f(\mathbf{x}_{\text{hi-fi}})$  with  $\mathbf{x}_{\text{hi-fi}} = (0.4 \text{ mm}, 1 \text{ ms})$  and in what follows we assess how well the GRE point estimate  $m_n[f](\mathbf{x}_{\text{hi-fi}})$  approximates  $f(\mathbf{x}_{\text{hi-fi}})$ . The central question here is whether the workflow proposed in Section 3.1 can provide more accurate approximation of  $f(\mathbf{x}_{\text{hi-fi}})$  compared to  $f(\mathbf{x}_{\text{default}})$ , and if so what computational budget is required. To the best of our knowledge there do not exist comparable methodologies for this task; methods such as emulation and MFM are not applicable when  $\boldsymbol{\theta}$  is fixed, and classical extrapolation methods were not developed with multivariate  $\mathbf{x}$  in mind.

The workflow is illustrated in the left panel of Figure 6. The lo-fi setting was  $\mathbf{x}_{\text{lo-fi}} = (1.7 \text{ mm}, 5 \text{ ms})$ . The convergence orders  $r_1, r_2$  were selected from  $\{0.5, 1, 2\}$ , the smoothness parameters  $s_1, s_2$  were selected from  $\{0, 1, 2\}$ , and the length-scales  $\ell_1, \ell_2$  were selected using grid search, all estimated simultaneously using maximum quasi-likelihood. Experimental designs were computed based on a candidate set of experiments, each of which incurs a cost no greater than  $c(\mathbf{x}_{\text{default}})$ , indicated by dots in the left panel of Figure 6. Rather than estimate the computational times, for this case study all candidate experiments were performed at the outset and their times recorded. Results for the 7 test problems are shown in the right panel of Figure 6, where it is observed that the GRE point estimator provides a

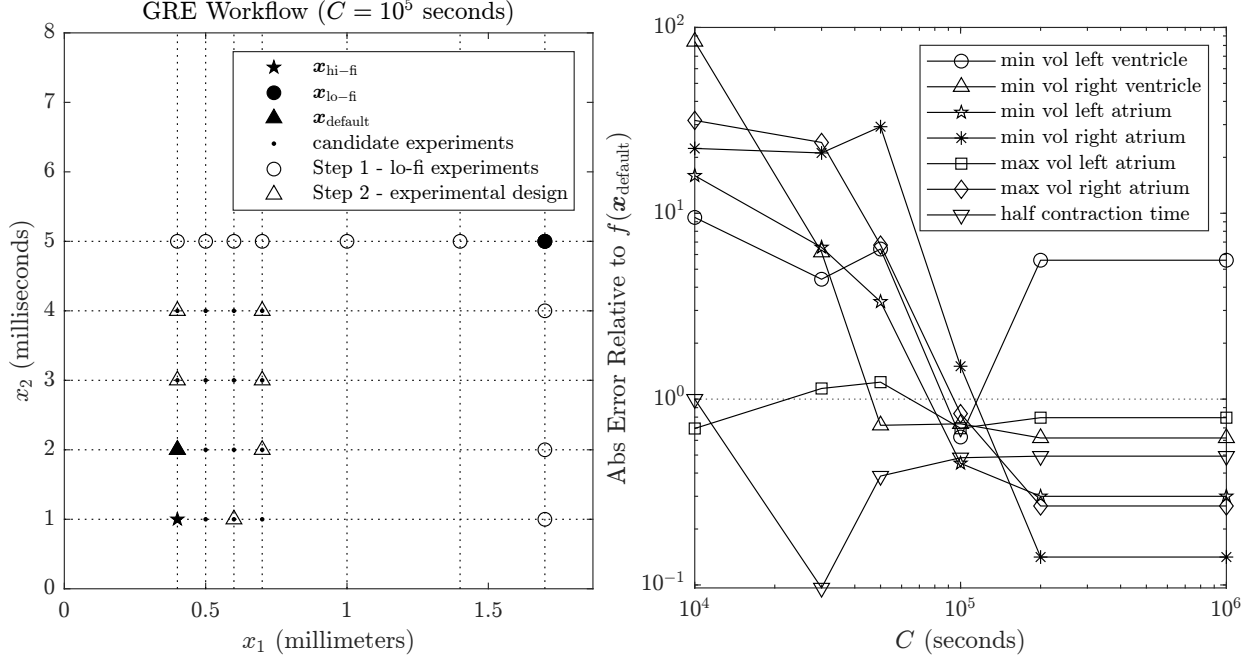


Figure 6: Scalar quantities of interest from the cardiac model. Left: The workflow, illustrated. In Step 1, the effect of varying each component of  $\mathbf{x}$  in turn is explored, with all other components fixed equal to their value in  $\mathbf{x}_{\text{lo-fi}}$ . This facilitates the construction of a multivariate Gaussian process model for use in Step 2, where experimental design is performed (here shown for a computational budget of  $C = 10^5$  seconds). For assessment purposes we aim to predict  $f(\mathbf{x}_{\text{hi-fi}})$  as a ground truth, but in practice the goal is to predict  $f(\mathbf{0})$ . Right: For each of the 7 scalar quantities of interest associated with the cardiac model we display the ratio of the absolute error  $|f(\mathbf{x}_{\text{hi-fi}}) - m_n[f](\mathbf{x}_{\text{hi-fi}})|$  of the GRE method and the absolute error  $|f(\mathbf{x}_{\text{hi-fi}}) - f(\mathbf{x}_{\text{default}})|$  of the default approximation, as a function of the total computational budget  $C$ .

generally better approximation to  $f(\mathbf{x}_{\text{hi-fi}})$  compared to  $f(\mathbf{x}_{\text{default}})$  when the computational budget  $C$  reaches or exceeds  $10^5$ . The optimal design for approximating the minimum volume of the left ventricle is depicted in the left hand panel of Figure 6 for a computational budget  $C = 10^5$ ; the design supplements  $\mathbf{x}_{\text{default}}$  with 6 additional simulations of lower cost, analogous to a classical extrapolation method but here generalised to the multivariate context. Note that for  $C$  exceeding  $2 \times 10^5$  the optimal design becomes saturated, containing all experiments in the candidate set. That GRE should perform worse than  $f(\mathbf{x}_{\text{default}})$  at small computational budgets is not surprising given that all convergence orders  $r_i$ , smoothnesses  $s_i$ , and length-scales  $\ell_i$  are estimated from the small lo-fi training dataset, and these values largely determine the output of GRE in the absence of a sufficient number of experiments in the training dataset  $X_n$ . However, for a sufficiently large computational budget, it is encouraging to see that information from the experiments in  $X_n$ , each of which cost no greater than  $c(\mathbf{x}_{\text{default}})$ , is exploited in GRE to achieve more accurate estimation for 6 of the



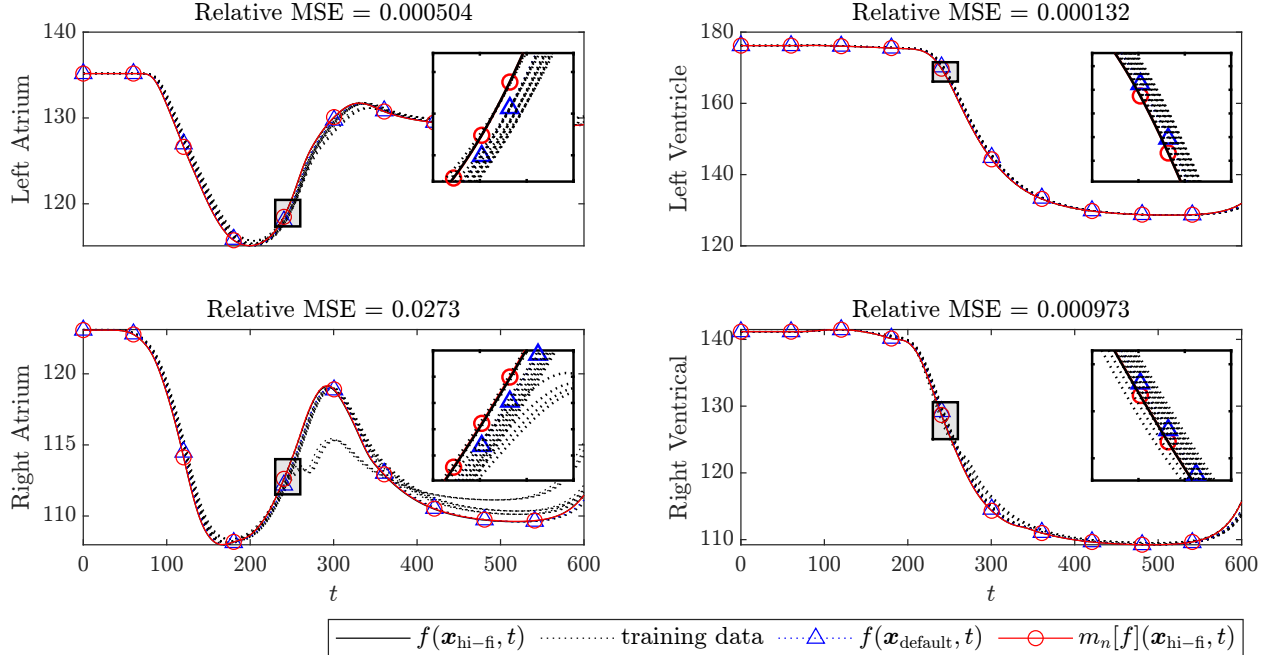


Figure 7: Temporal quantities of interest from the cardiac model. For each of the 4 temporal quantities of interest associated with the cardiac model we display the approximations produced at the different spatial and temporal resolutions in the training dataset  $X_n$ , together with the ground truth  $f(\mathbf{x}_{\text{hi-fi}})$  (solid black lines), the default approximation  $f(\mathbf{x}_{\text{default}}, t)$  (blue triangles), and the approximation  $m_n[f](\mathbf{x}_{\text{hi-fi}}, t)$  from Gauss–Richardson Extrapolation (GRE; red circles). The ratio of the mean square error  $\int [f(\mathbf{x}_{\text{hi-fi}}, t) - m_n[f](\mathbf{x}_{\text{hi-fi}}, t)]^2 dt$  of the GRE method and the mean square error  $\int [f(\mathbf{x}_{\text{hi-fi}}, t) - f(\mathbf{x}_{\text{default}}, t)]^2 dt$  of the default method is also reported.

7 scalar quantities of interest.

### 3.3 Approximation of Temporal Model Output

The scalar quantities of interest considered in Section 3.2 are summary statistics obtained from 4-dimensional temporal model output of the form  $\mathbf{f}(\mathbf{x}, t)$ , where here  $t$  is a time index ranging from 0 to 600 ms and the components of  $\mathbf{f}$  refer to the volumes of the atria and ventricles. It is therefore interesting to investigate whether these temporal outputs can be directly approximated, providing 4 test problems for the methodology described in Section 2.9. Here for simplicity we fixed the discrete values  $s_1, s_2, r_1,$  and  $r_2$ , the median of the values estimated in Section 3.2, and we fixed the continuous values  $\hat{\sigma}_1, \hat{\sigma}_2, \ell_1,$  and  $\ell_2$  to the mean of the values estimated in Section 3.2. The length-scale for the kernel  $k_{\mathcal{T}}$  was set equal to the length of the time series itself. The computational budget was fixed to  $C = 2 \times 10^5$ , so that our experimental design is saturated, but recall that no individual experiment in this design had cost exceeding  $c(\mathbf{x}_{\text{default}})$ . Full results are displayed in Figure 7. In each case the

approximation produced by GRE achieves lower mean square error relative to  $f(\mathbf{x}_{\text{default}}, t)$ . Taken together with the results in Section 3.2, these results are an encouraging and pave the way for subsequent investigations and applications of GRE.

## 4 Discussion

This paper introduced a probabilistic perspective on extrapolation, presenting a framework in which classical extrapolation methods from numerical analysis and modern multi-fidelity modelling are unified. One approach was developed in detail, which we termed *Gauss–Richardson Extrapolation* (GRE). The GRE method facilitates simultaneous convergence acceleration and uncertainty quantification, and unlocks experimental design functionality for optimisation over the set of fidelities at which simulation is performed. The end result is a methodology that allows a practitioner to arrive, in a principled manner, at fidelities  $\{\mathbf{x}_i\}_{i=1}^n$  such that the associated simulator outputs  $\{f(\mathbf{x}_i)\}_{i=1}^n$  can be combined to produce an approximation to the continuum quantity  $f(\mathbf{0})$  that is typically more accurate than a single hi-fi simulation run at a comparable computational cost. A cardiac modelling case study provided an initial positive proof-of-concept, but further case studies – involving different types of computer model – will be required to comprehensively assess GRE; we aim to undertake domain-specific investigations in future work.

Several methodological extensions to this work can be envisaged, such as considering alternative regression models to GPs, developing theory and methodology for the more challenging cases where the regression model is misspecified and computational costs needs to be predicted, and extending the experimental design methodology to include additional degrees of freedom  $\boldsymbol{\theta}$ , which are often present in a mathematical model. In addition, and more speculatively, it would be interesting to explore modern computational tasks, such as the super-resolution task in deep learning, for which extrapolation methods have yet to be exploited.

**Acknowledgements** The authors wish to thank Onur Teymur and Jere Koskela for early discussions of this project. CJO was supported by EP/W019590/1 and a Leverhulme Prize. TK was supported by the Research Council of Finland postdoctoral researcher grant number 338567, *Scalable, Adaptive and Reliable Probabilistic Integration*. ALT was supported by EP/X01259X/1 and EP/R014604/1. CJO and ALT would like to thank the Isaac Newton Institute for Mathematical Sciences, Cambridge, for support and hospitality during the programme *Mathematical and Statistical Foundation of Future Data-Driven Engineering* where work on this paper was undertaken. MS and SAN were supported by the Wellcome/EPSRC Centre for Medical Engineering (WT203148/Z/16/Z). SAN was supported by NIH R01-HL152256, ERC PREDICT-HF 453 (864055), BHF (RG/20/4/34803), and EPSRC (EP/P01268X/1, EP/X03870X/1).

## References

- C. P. Arroyo, J. Dombard, F. Duchaine, L. Gicquel, B. Martin, N. Odier, and G. Staffelbach. Towards the large-eddy simulation of a full engine: Integration of a 360 azimuthal degrees fan, compressor and combustion chamber. Part I: Methodology and initialisation. *Journal of the Global Power and Propulsion Society*, page 133115, 2021.
- C. M. Augustin, M. A. Gsell, E. Karabelas, E. Willemen, F. W. Prinzen, J. Lumens, E. J. Vigmond, and G. Plank. A computationally efficient physiologically comprehensive 3D–0D closed-loop model of the heart and circulation. *Computer Methods in Applied Mechanics and Engineering*, 386:114092, 2021.
- F. Bach. On the effectiveness of Richardson extrapolation in data science. *SIAM Journal on Mathematics of Data Science*, 3(4):1251–1277, 2021.
- J. D. Bayer, R. C. Blake, G. Plank, and N. A. Trayanova. A novel rule-based algorithm for assigning myocardial fiber orientation to computational heart models. *Annals of Biomedical Engineering*, 40:2243–2254, 2012.
- A. Berlinet and C. Thomas-Agnan. *Reproducing Kernel Hilbert Spaces in Probability and Statistics*. Springer Science & Business Media, 2011.
- C. A. Beschle and A. Barth. Quasi continuous level Monte Carlo for random elliptic PDEs. *arXiv preprint arXiv:2303.08694*, 2023.
- C. Brezinski. Composite sequence transformations. *Numerische Mathematik*, 46:311–321, 1985.
- C. Brezinski. A survey of iterative extrapolation by the E-algorithm, Det Kong. *Det Kongelige Norske Videnskabers Selskabs Skrifter*, 2:1–26, 1989.
- C. Brezinski and M. R. Zaglia. *Extrapolation Methods: Theory and Practice*. Elsevier, 2013.
- R. Bulirsch and J. Stoer. Fehlerabschätzungen und Extrapolation mit rationalen Funktionen bei Verfahren vom Richardson-Typus. *Numerische Mathematik*, 6(1):413–427, 1964.
- V. Cabannes and S. Vigogna. How many samples are needed to leverage smoothness? *arXiv preprint arXiv:2305.16014*, 2023.
- L. Chizat, P. Roussillon, F. Léger, F.-X. Vialard, and G. Peyré. Faster Wasserstein distance estimation with the Sinkhorn divergence. *Advances in Neural Information Processing Systems*, 33:2257–2269, 2020.
- J. Cockayne, C. J. Oates, T. J. Sullivan, and M. Girolami. Bayesian probabilistic numerical methods. *SIAM Review*, 61(4):756–789, 2019.

- P. S. Craig, M. Goldstein, A. Seheult, and J. Smith. Constructing partial prior specifications for models of complex physical systems. *Journal of the Royal Statistical Society, Series D*, 47(1):37–53, 1998.
- J. A. Cumming and M. Goldstein. Small sample Bayesian designs for complex high-dimensional models based on information gained using fast approximations. *Technometrics*, 51(4):377–388, 2009.
- J.-P. Delahaye. Automatic selection of sequence transformations. *Mathematics of Computation*, 37(155):197–204, 1981.
- A. Durmus, U. Simsekli, E. Moulines, R. Badeau, and G. Richard. Stochastic gradient Richardson-Romberg Markov chain Monte Carlo. *Advances in Neural Information Processing Systems*, 29, 2016.
- A. Ehara and S. Guillas. An adaptive strategy for sequential designs of multilevel computer experiments. *International Journal for Uncertainty Quantification*, 13(4), 2023.
- B. Germain-Bonne. Convergence acceleration of number-machine sequences. *Journal of Computational and Applied Mathematics*, 32(1-2):83–88, 1990.
- J. Han, A. Jentzen, and W. E. Solving high-dimensional partial differential equations using deep learning. *Proceedings of the National Academy of Sciences*, 115(34):8505–8510, 2018.
- A. Hansson, M. Holm, P. Blomström, R. Johansson, C. Lührs, J. Brandt, and S. Olsson. Right atrial free wall conduction velocity and degree of anisotropy in patients with stable sinus rhythm studied during open heart surgery. *European Heart Journal*, 19(2):293–300, 1998.
- I. M. Held. The gap between simulation and understanding in climate modeling. *Bulletin of the American Meteorological Society*, 86(11):1609–1614, 2005.
- P. Hennig, M. A. Osborne, and M. Girolami. Probabilistic numerics and uncertainty in computations. *Proceedings of the Royal Society A: Mathematical, Physical and Engineering Sciences*, 471(2179):20150142, 2015.
- P. E. Jacob, J. O’Leary, and Y. F. Atchadé. Unbiased Markov chain Monte Carlo methods with couplings. *Journal of the Royal Statistical Society, Series B*, 82(3):543–600, 2020.
- Y. Ji, H. S. Yuchi, D. Soeder, J.-F. Paquet, S. A. Bass, V. R. Joseph, C. F. J. Wu, and S. Mak. Conglomerate multi-fidelity Gaussian process modeling, with application to heavy-ion collisions. *arXiv preprint arXiv:2209.13748*, 2022.
- T. Karvonen. Small sample spaces for Gaussian processes. *Bernoulli*, 29(2):875–900, 2023.
- T. Karvonen, C. J. Oates, and S. Särkkä. A Bayes–Sard cubature method. *Advances in Neural Information Processing Systems*, 31:5882–5893, 2018.

- T. Karvonen, G. Wynne, F. Tronarp, C. Oates, and S. Sarkka. Maximum likelihood estimation and uncertainty quantification for Gaussian process approximation of deterministic functions. *SIAM/ASA Journal on Uncertainty Quantification*, 8(3):926–958, 2020.
- M. C. Kennedy and A. O’Hagan. Predicting the output from a complex computer code when fast approximations are available. *Biometrika*, 87(1):1–13, 2000.
- F. Larkin. Some techniques for rational interpolation. *The Computer Journal*, 10(2):178–187, 1967.
- M. Ledoux and M. Talagrand. *Probability in Banach Spaces: Isoperimetry and Processes*. Springer Science & Business Media, 1991.
- V. Lemaire and G. Pagès. Multilevel Richardson–Romberg extrapolation. *Bernoulli*, 20(3):1029–1067, 2017.
- D. J. Lucia, P. S. Beran, and W. A. Silva. Reduced-order modeling: New approaches for computational physics. *Progress in Aerospace Sciences*, 40(1-2):51–117, 2004.
- W. Madych and S. Nelson. Bounds on multivariate polynomials and exponential error estimates for multiquadric interpolation. *Journal of Approximation Theory*, 70(1):94–114, 1992.
- A. J. Majda and B. Gershgorin. Quantifying uncertainty in climate change science through empirical information theory. *Proceedings of the National Academy of Sciences*, 107(34):14958–14963, 2010.
- H. Mhaskar, F. Narcowich, and J. Ward. Spherical Marcinkiewicz-Zygmund inequalities and positive quadrature. *Mathematics of Computation*, 70(235):1113–1130, 2001.
- A. Neic, F. O. Campos, A. J. Prassl, S. A. Niederer, M. J. Bishop, E. J. Vigmond, and G. Plank. Efficient computation of electrograms and ECGs in human whole heart simulations using a reaction-eikonal model. *Journal of Computational Physics*, 346:191–211, 2017.
- A. Neic, M. A. Gsell, E. Karabelas, A. J. Prassl, and G. Plank. Automating image-based mesh generation and manipulation tasks in cardiac modeling workflows using meshtool. *SoftwareX*, 11:100454, 2020.
- S. A. Niederer, G. Plank, P. Chinchapatnam, M. Ginks, P. Lamata, K. S. Rhode, C. A. Rinaldi, R. Razavi, and N. P. Smith. Length-dependent tension in the failing heart and the efficacy of cardiac resynchronization therapy. *Cardiovascular Research*, 89(2):336–343, 2011.
- N. Ono, T. Yamaguchi, H. Ishikawa, M. Arakawa, N. Takahashi, T. Saikawa, and T. Shimada. Morphological varieties of the purkinje fiber network in mammalian hearts, as revealed by light and electron microscopy. *Archives of Histology and Cytology*, 72(3):139–149, 2009.

- V. I. Paulsen and M. Raghupathi. *An Introduction to the Theory of Reproducing Kernel Hilbert Spaces*. Cambridge University Press, 2016.
- B. Peherstorfer, K. Willcox, and M. Gunzburger. Survey of multifidelity methods in uncertainty propagation, inference, and optimization. *SIAM Review*, 60(3):550–591, 2018.
- P. Piperni, A. DeBlois, and R. Henderson. Development of a multilevel multidisciplinary-optimization capability for an industrial environment. *AIAA Journal*, 51(10):2335–2352, 2013.
- E. Porcu, M. Bevilacqua, R. Schaback, and C. J. Oates. The Matérn model: A journey through statistics, numerical analysis and machine learning. *Statistical Science*, 2024. To appear.
- C. E. Rasmussen and C. K. Williams. *Gaussian Processes for Machine Learning*. Springer, 2006.
- C.-H. Rhee and P. W. Glynn. Unbiased estimation with square root convergence for SDE models. *Operations Research*, 63(5):1026–1043, 2015.
- L. F. Richardson. The approximate arithmetical solution by finite differences of physical problems involving differential equations, with an application to the stresses in a masonry dam. *Philosophical Transactions of the Royal Society A*, 210(459-470):307–357, 1911.
- L. F. Richardson and J. A. Gaunt. The deferred approach to the limit. *Philosophical Transactions of the Royal Society A*, 226:223–361, 1927.
- C. H. Roney, A. Pashaei, M. Meo, R. Dubois, P. M. Boyle, N. A. Trayanova, H. Cochet, S. A. Niederer, and E. J. Vigmond. Universal atrial coordinates applied to visualisation, registration and construction of patient specific meshes. *Medical Image Analysis*, 55:65–75, 2019.
- J. Sacks, W. J. Welch, T. J. Mitchell, and H. P. Wynn. Design and analysis of computer experiments. *Statistical Science*, 4(4):409–423, 1989.
- D. Shanks. Non-linear transformations of divergent and slowly convergent sequences. *Journal of Mathematics and Physics*, 34(1-4):1–42, 1955.
- A. Sidi. *Practical Extrapolation Methods: Theory and Applications*. Cambridge University Press, 2003.
- M. L. Stein. *Interpolation of Spatial Data: Some Theory for Kriging*. Springer Science & Business Media, 1999.
- M. L. Stein and Y. Hung. Comment on “Probabilistic integration: A role in statistical computation?”. *Statistical Science*, 34(1):34–37, 2019.

- M. Strocchi, M. A. Gsell, C. M. Augustin, O. Razeghi, C. H. Roney, A. J. Prassl, E. J. Vigmond, J. M. Behar, J. S. Gould, C. A. Rinaldi, et al. Simulating ventricular systolic motion in a four-chamber heart model with spatially varying robin boundary conditions to model the effect of the pericardium. *Journal of Biomechanics*, 101:109645, 2020.
- M. Strocchi, S. Longobardi, C. M. Augustin, M. A. Gsell, A. Petras, C. A. Rinaldi, E. J. Vigmond, G. Plank, C. J. Oates, R. D. Wilkinson, et al. Cell to whole organ global sensitivity analysis on a four-chamber heart electromechanics model using Gaussian processes emulators. *PLOS Computational Biology*, 19(6):e1011257, 2023.
- P. Taggart, P. M. Sutton, T. Opthof, R. Coronel, R. Trimlett, W. Pugsley, and P. Kallis. Inhomogeneous transmural conduction during early ischaemia in patients with coronary artery disease. *Journal of Molecular and Cellular Cardiology*, 32(4):621–630, 2000.
- O. Teymur, C. Foley, P. Breen, T. Karvonen, and C. J. Oates. Black box probabilistic numerics. *Advances in Neural Information Processing Systems*, 34:23452–23464, 2021.
- T. N. Thiele. *Interpolationsrechnung*. BG Teubner, 1909.
- P. Thodoroff, M. Kaiser, R. Williams, R. Arthern, S. Hosking, N. Lawrence, J. Byrne, and I. Kazlauskaite. Multi-fidelity experimental design for ice-sheet simulation. *arXiv preprint arXiv:2307.08449*, 2023.
- R. Tuo, C. J. Wu, and D. Yu. Surrogate modeling of computer experiments with different mesh densities. *Technometrics*, 56(3):372–380, 2014.
- E. J. Vigmond, M. Hughes, G. Plank, and L. J. Leon. Computational tools for modeling electrical activity in cardiac tissue. *Journal of Electrocardiology*, 36:69–74, 2003.
- H. Wendland. *Scattered Data Approximation*. Cambridge University Press, 2004.

# Appendices

---

<b>A Kernels and Smoothness Spaces</b>	<b>32</b>
<b>B Proofs of Results in the Main Text</b>	<b>33</b>
B.1 Sample Path Properties of Numerical Analysis-Informed GPs . . . . .	33
B.2 Derivation of the ‘Objective’ Prior Limit . . . . .	35
B.3 Technical Results on Polynomial Reproduction . . . . .	36
B.4 Proof of Theorem 2 . . . . .	38
B.5 Proof of Theorem 4 . . . . .	40
B.6 Verifying the Assumptions for Example 5 . . . . .	41
B.7 Proof of Proposition 6 and Corollary 7 . . . . .	42
B.8 Proof of Proposition 9 . . . . .	42
B.9 Proof of Proposition 12 . . . . .	44
B.10 Calculations for Multidimensional Output . . . . .	45
<b>C Details for the Cardiac Model</b>	<b>46</b>

---

## A Kernels and Smoothness Spaces

This appendix contains definitions for the kernels  $k_e : \mathcal{X} \times \mathcal{X} \rightarrow \mathbb{R}$ , on a bounded set  $\mathcal{X} \subset \mathbb{R}^d$ , referred to in the main text, together with details about the smoothness of elements in the Hilbert spaces  $\mathcal{H}_{k_e}(\mathcal{X})$  that are reproduced. All kernels  $k_e$  that we discussed take the radial form

$$k_e(\mathbf{x}, \mathbf{y}) = \phi(d_{\boldsymbol{\ell}}(\mathbf{x}, \mathbf{y})), \quad d_{\boldsymbol{\ell}}(\mathbf{x}, \mathbf{y}) = \left( \sum_{i=1}^d \frac{(x_i - y_i)^2}{\ell_i^2} \right)^{1/2},$$

where the radial function  $\phi : [0, \infty) \rightarrow \mathbb{R}$  and the length-scale parameters  $\boldsymbol{\ell} \in (0, \infty)^d$  are to be specified.

**Matern Kernels** The Matern family of kernels is defined via the radial function

$$\phi_{\nu}(z) = \exp\left(-\sqrt{2s+1} z\right) \frac{s!}{(2s)!} \sum_{i=0}^s \frac{(s+i)!}{i!(s-i)!} \left(2\sqrt{2s+1} z\right)^{s-i}$$



for which  $k_e \in C^{2s}(\mathcal{X} \times \mathcal{X})$  (Stein, 1999, Section 2.7). The kernel  $k_e$  reproduces (up to an equivalent norm) the Sobolev space  $H^{s+\frac{d+1}{2}}(\mathcal{X})$  (Wendland, 2004, Corollary 10.48). The elements of  $H^{s+\frac{d+1}{2}}(\mathcal{X})$  are functions whose mixed weak partial derivatives up to order  $s+\frac{d+1}{2}$  exist as elements of  $L^2(\mathcal{X})$ , and so in particular  $C^{s+\frac{d+1}{2}}(\mathcal{X}) \subset H^{s+\frac{d+1}{2}}(\mathcal{X})$ . Conversely, from the Sobolev embedding theorem,  $H^{s+\frac{d+1}{2}}(\mathcal{X}) \subset C^s(\mathcal{X})$ . Thus  $C^{s+\frac{d+1}{2}}(\mathcal{X}) \subset \mathcal{H}_{k_e}(\mathcal{X}) \subset C^s(\mathcal{X})$ . It may be helpful to point out that, somewhat confusingly, in most of the statistical literature the Matérn kernel is defined in terms of a ‘smoothness parameter’  $\nu := s + \frac{1}{2}$  (Porcu et al., 2024). From Section 2.4 of this paper onward, “Matérn ( $s = m$ )” refers to  $\phi_\nu$  with  $\nu = m + \frac{1}{2}$ . As an example, the Matérn- $\frac{5}{2}$  kernel that appears in Figure 1 would correspond to  $s = 2$  in our framework.

**Wendland Kernels** Let  $z_+^m := \max(0, z)^m$  and  $(\mathcal{I}\varphi)(z) := \int_z^\infty t\varphi(t) dt$ . The Wendland family of kernels is defined via the radial function

$$\phi_{d,s}(z) = \mathcal{I}^s \varphi_{[\frac{d}{2}]_+ + s + 1}(z), \quad \varphi_m(z) = (1 - z)_+^m$$

for  $s \in \mathbb{N}_0$ , for which  $k_e \in C^{2s}(\mathcal{X} \times \mathcal{X})$ ; see Theorem 9.13 of Wendland (2004). The kernel  $k_e$  reproduces (up to an equivalent norm) the Sobolev space  $H^{s+\frac{d+1}{2}}(\mathcal{X})$ , at least when  $s \geq 1$  (for  $s = 0$  we need  $d \geq 3$ ); see Theorem 10.35 of Wendland (2004). Thus again  $C^{s+\frac{d+1}{2}}(\mathcal{X}) \subset \mathcal{H}_{k_e}(\mathcal{X}) \subset C^s(\mathcal{X})$ . Wendland kernels are sometimes preferred to Matérn kernels due to their compact support (but they are not the only available alternative with compact support; Porcu et al., 2024).

**Gaussian Kernels** More generally, if the kernel  $k_e$  satisfies  $k_e \in C^{2s}(\mathcal{X} \times \mathcal{X})$  with  $\mathcal{X}$  an open subset of  $\mathbb{R}^d$ , then  $\mathcal{H}_{k_e}(\mathcal{X}) \subset C^s(\mathcal{X})$ ; see Theorem 10.45 of Wendland (2004). In particular the Gaussian kernel, defined by the radial function

$$\phi(z) = \exp(-z^2),$$

has continuous derivatives of all orders, so elements of the associated Hilbert space are  $C^\infty(\mathcal{X})$ .

## B Proofs of Results in the Main Text

This appendix contains proofs for all theoretical results presented in the main text.

### B.1 Sample Path Properties of Numerical Analysis-Informed GPs

This appendix presents sufficient conditions under which sample paths  $g$  from the numerical analysis-informed GP in (3) satisfy, with probability one,  $g(\mathbf{x}) - g(\mathbf{0}) = O(b(\mathbf{x}))$  in the  $\mathbf{x} \rightarrow \mathbf{0}$  limit. To be precise, we establish that there is a *version*  $g$  of  $\mathcal{GP}(0, k)$  for which, with probability one,  $g(\mathbf{x}) - g(\mathbf{0}) = O(b(\mathbf{x}))$ . Recall that a stochastic process  $h$  is said to be a *version* of  $g$  if  $h(\mathbf{x}) = g(\mathbf{x})$  with probability one, for all  $\mathbf{x} \in \mathcal{X} \setminus \{\mathbf{0}\}$ . This technical

consideration arises simply because stochastic processes can be altered on null sets, affecting their convergence properties while leaving their distribution unchanged.

**Proposition 13** (Sample paths of numerical analysis-informed GPs). *In the setting of Section 2.1, assume that  $k_e$  is Hölder continuous for some exponent; i.e. there exist  $C, \alpha > 0$  such that  $|k_e(\mathbf{x}, \mathbf{x}) - k_e(\mathbf{x}, \mathbf{x}')| \leq C\|\mathbf{x} - \mathbf{x}'\|^\alpha$  for all  $\mathbf{x}, \mathbf{x}' \in \mathcal{X}$ , and that the set  $\mathcal{X}$  is bounded. Then there is a version  $g$  of  $\mathcal{GP}(0, k)$  for which, with probability one,  $g(\mathbf{x}) - g(\mathbf{0}) = O(b(\mathbf{x}))$  in the  $\mathbf{x} \rightarrow \mathbf{0}$  limit.*

*Proof.* Let  $e(\mathbf{x}) := b(\mathbf{x})^{-1}(g(\mathbf{x}) - g(\mathbf{0}))$  for  $\mathbf{x} \in \mathcal{X} \setminus \{\mathbf{0}\}$ , which is well-defined since  $b(\mathbf{x}) > 0$  for all  $\mathbf{x} \in \mathcal{X} \setminus \{\mathbf{0}\}$ . From (3), if  $g \sim \mathcal{GP}(0, k)$  then the distribution of  $e$  is  $\mathcal{GP}(0, k_e|_{\mathcal{X} \setminus \{\mathbf{0}\}})$ , where  $k_e|_{\mathcal{X} \setminus \{\mathbf{0}\}}(\mathbf{x}, \mathbf{x}') = k_e(\mathbf{x}, \mathbf{x}')$  for all  $\mathbf{x}, \mathbf{x}' \in \mathcal{X} \setminus \{\mathbf{0}\}$ . Our task is equivalent to establishing that there is a version of  $e$  for which  $e(\mathbf{x})$  is almost surely bounded as  $\mathbf{x} \rightarrow \mathbf{0}$ , but we will in fact establish the stronger result that there is a version of  $e$  for which  $\mathbb{P}(\sup_{\mathbf{x} \in \mathcal{X} \setminus \{\mathbf{0}\}} |e(\mathbf{x})| < \infty) = 1$ . From Markov's inequality, this follows if  $\mathbb{E}[\sup_{\mathbf{x} \in \mathcal{X} \setminus \{\mathbf{0}\}} |e(\mathbf{x})|] < \infty$ , and in fact it is sufficient to show that

$$\mathbb{E} \left[ \sup_{\mathbf{x} \in \mathcal{X} \setminus \{\mathbf{0}\}} e(\mathbf{x}) \right] < \infty. \quad (12)$$

Indeed, for any  $\mathbf{x}_0 \in \mathcal{X} \setminus \{\mathbf{0}\}$ , we have

$$\begin{aligned} |e(\mathbf{x})| &\leq |e(\mathbf{x}_0)| + |e(\mathbf{x}) - e(\mathbf{x}_0)| \\ &\leq |e(\mathbf{x}_0)| + \sup_{\mathbf{x}' \in \mathcal{X} \setminus \{\mathbf{0}\}} [e(\mathbf{x}') - e(\mathbf{x}_0)] - \inf_{\mathbf{x}' \in \mathcal{X} \setminus \{\mathbf{0}\}} [e(\mathbf{x}') - e(\mathbf{x}_0)] \end{aligned}$$

from which it follows that

$$\begin{aligned} \mathbb{E} \left[ \sup_{\mathbf{x} \in \mathcal{X} \setminus \{\mathbf{0}\}} |e(\mathbf{x})| \right] &\leq \mathbb{E}[|e(\mathbf{x}_0)|] + \mathbb{E} \left[ \sup_{\mathbf{x}' \in \mathcal{X} \setminus \{\mathbf{0}\}} e(\mathbf{x}') - e(\mathbf{x}_0) \right] - \mathbb{E} \left[ \inf_{\mathbf{x}' \in \mathcal{X} \setminus \{\mathbf{0}\}} e(\mathbf{x}') - e(\mathbf{x}_0) \right] \\ &= \mathbb{E}[|e(\mathbf{x}_0)|] + 2\mathbb{E} \left[ \sup_{\mathbf{x}' \in \mathcal{X} \setminus \{\mathbf{0}\}} e(\mathbf{x}') \right], \end{aligned}$$

where  $\mathbb{E}[|e(\mathbf{x}_0)|] < \infty$  since  $e(\mathbf{x}_0)$  is Gaussian, and where the final equality followed from  $\mathbb{E}[e(\mathbf{x}_0)] = 0$  and symmetry of the GP.

Our main tools to establish (12) are entropy numbers and Dudley's theorem. The Hölder condition ensures that the induced pseudometric  $\mathbf{d} : \mathcal{X} \times \mathcal{X} \rightarrow [0, \infty)$  defined via  $\mathbf{d}(\mathbf{x}, \mathbf{x}')^2 := k_e(\mathbf{x}, \mathbf{x}) - 2k_e(\mathbf{x}, \mathbf{x}') + k_e(\mathbf{x}', \mathbf{x}')$  satisfies  $\mathbf{d}(\mathbf{x}, \mathbf{x}') \leq \sqrt{2C}\|\mathbf{x} - \mathbf{x}'\|^{\alpha/2}$  for all  $\mathbf{x}, \mathbf{x}' \in \mathcal{X}$ . Let  $B_{\epsilon, \mathbf{d}}(\mathbf{x}) := \{\mathbf{x}' \in \mathcal{X} \setminus \{\mathbf{0}\} : \mathbf{d}(\mathbf{x}, \mathbf{x}') < \epsilon\}$  denote an open  $\mathbf{d}$ -ball of radius  $\epsilon$  centred at  $\mathbf{x}$ , and let  $N(\mathcal{X} \setminus \{\mathbf{0}\}, \mathbf{d}; \epsilon)$  denote the *entropy number*; the minimal number of open  $\mathbf{d}$ -balls of radius  $\epsilon$  required to cover  $\mathcal{X} \setminus \{\mathbf{0}\}$ . The boundedness condition on  $\mathcal{X}$  ensures that the entropy number is well-defined. Dudley's theorem states that, in our context, there is a version  $e$  of  $\mathcal{GP}(0, k_e)$  such that

$$\mathbb{E} \left[ \sup_{\mathbf{x} \in \mathcal{X} \setminus \{\mathbf{0}\}} e(\mathbf{x}) \right] \leq 24 \int_0^\infty \sqrt{\log N(\mathcal{X} \setminus \{\mathbf{0}\}, \mathbf{d}; \epsilon)} \, d\epsilon; \quad (13)$$

see Theorem 11.17 in Ledoux and Talagrand (1991). Our task is now to establish that the integral in (13) is finite, and to this end we make use of a simple upper bound on the entropy number for  $\mathbf{d}$  in terms of the entropy number for the usual Euclidean distance  $\mathbf{e}(\mathbf{x}, \mathbf{x}') := \|\mathbf{x} - \mathbf{x}'\|$  by noting that

$$\begin{aligned} B_{\epsilon, \mathbf{d}}(\mathbf{x}) &= \{\mathbf{x}' \in \mathcal{X} \setminus \{\mathbf{0}\} : \mathbf{d}(\mathbf{x}, \mathbf{x}') < \epsilon\} \\ &\supseteq \{\mathbf{x}' \in \mathcal{X} \setminus \{\mathbf{0}\} : \sqrt{2C}\|\mathbf{x} - \mathbf{x}'\|^{\alpha/2} < \epsilon\} = B_{(\epsilon/C)^{1/\alpha}, \mathbf{e}}(\mathbf{x}), \end{aligned}$$

from which it follows that  $N(\mathcal{X} \setminus \{\mathbf{0}\}, \mathbf{d}; \epsilon) \leq N(\mathcal{X} \setminus \{\mathbf{0}\}, \mathbf{e}; (\epsilon/C)^{1/\alpha})$ . Since  $\mathcal{X}$  is bounded, the entropy number for the Euclidean distance can be bounded by considering the number of Euclidean balls of radius  $(\epsilon/C)^{1/\alpha}$  that are needed to cover a sufficiently large cube in  $\mathbb{R}^d$ , from which we obtain a bound of the form

$$N\left(\mathcal{X} \setminus \{\mathbf{0}\}, \mathbf{e}; \left(\frac{\epsilon}{C}\right)^{1/\alpha}\right) \leq \max\left\{1, \tilde{C} \left(\frac{C}{\epsilon}\right)^{d/\alpha}\right\}$$

for some constant  $\tilde{C}$ , from which the finiteness of the integral in (13) can be established. Indeed, letting  $\epsilon_0 = \tilde{C}^{\alpha/d} C$ , we have the bound

$$\begin{aligned} \int_0^\infty \sqrt{\log N(\mathcal{X}, \mathbf{d}; \epsilon)} \, \mathrm{d}\epsilon &\leq \int_0^\infty \sqrt{\max\left\{0, \frac{d}{\alpha} \log\left(\frac{\epsilon_0}{\epsilon}\right)\right\}} \, \mathrm{d}\epsilon \\ &= \sqrt{\frac{d}{\alpha}} \int_0^{\epsilon_0} \sqrt{\log\left(\frac{\epsilon_0}{\epsilon}\right)} \, \mathrm{d}\epsilon = \sqrt{\frac{\pi d}{\alpha}} \frac{\epsilon_0}{2} < \infty, \end{aligned}$$

as required.  $\square$

The Hölder and boundedness assumptions in Proposition 6 are weak and hold for all of the examples in this paper that we considered.

## B.2 Derivation of the ‘Objective’ Prior Limit

This appendix contains standard calculations that can be found in references such as Karvonen et al. (2018), but we include them here to keep the paper self-contained. Let  $f \sim \mathcal{GP}(0, k)$  where we fix finite values of  $\sigma^2, k_0^2 > 0$  in the specification of  $k$  in (3). The distribution of  $f$  conditional upon the components  $f(X_n)$  takes the familiar form

$$m_n[f](\mathbf{x}) = \mathbf{k}(\mathbf{x})^\top \mathbf{K}^{-1} f(X_n), \quad (14)$$

$$k_n[f](\mathbf{x}, \mathbf{x}') = k(\mathbf{x}, \mathbf{x}') - \mathbf{k}(\mathbf{x})^\top \mathbf{K}^{-1} \mathbf{k}(\mathbf{x}'); \quad (15)$$

see Chapter 2 of Rasmussen and Williams (2006). Here  $k(\mathbf{x}, \mathbf{x}') = \sigma^2\{k_0^2 + k_b(\mathbf{x}, \mathbf{x}')\}$ ,  $\mathbf{k}(\mathbf{x}) = \sigma^2\{k_0^2 \mathbf{1} + \mathbf{k}_b(\mathbf{x})\}$ , and  $\mathbf{K} = \sigma^2\{k_0^2 \mathbf{1}\mathbf{1}^\top + \mathbf{K}_b\}$ . Next we use the Woodbury matrix inversion identity to deduce that

$$\mathbf{K}^{-1} = \sigma^{-2}(k_0^2 \mathbf{1}\mathbf{1}^\top + \mathbf{K}_b)^{-1} = \sigma^{-2}\{\mathbf{K}_b^{-1} - \mathbf{K}_b^{-1} \mathbf{1}(k_0^{-2} + \mathbf{1}^\top \mathbf{K}_b^{-1} \mathbf{1})^{-1} \mathbf{1}^\top \mathbf{K}_b^{-1}\}. \quad (16)$$

Plugging this into (14) and (15), we obtain

$$\begin{aligned} m_n[f](\mathbf{x}) &= \{k_0^2 \mathbf{1} + \mathbf{k}_b(\mathbf{x})\}^\top \{\mathbf{K}_b^{-1} - \mathbf{K}_b^{-1} \mathbf{1} (k_0^{-2} + \mathbf{1}^\top \mathbf{K}_b^{-1} \mathbf{1})^{-1} \mathbf{1}^\top \mathbf{K}_b^{-1}\} f(X_n), \\ \frac{k_n[f](\mathbf{x}, \mathbf{x}')}{\sigma^2} &= k_0^2 + k_b(\mathbf{x}, \mathbf{x}') - (k_0^2 \mathbf{1} + \mathbf{k}_b(\mathbf{x}))^\top \left\{ \mathbf{K}_b^{-1} - \frac{\mathbf{K}_b^{-1} \mathbf{1} \mathbf{1}^\top \mathbf{K}_b^{-1}}{(k_0^{-2} + \mathbf{1}^\top \mathbf{K}_b^{-1} \mathbf{1})} \right\} (k_0^2 \mathbf{1} + \mathbf{k}_b(\mathbf{x}')). \end{aligned} \quad (17)$$

Then, for small  $k_0^{-2}$ , we have from a Taylor expansion that

$$(k_0^{-2} + \mathbf{1}^\top \mathbf{K}_b^{-1} \mathbf{1})^{-1} = \frac{1}{\mathbf{1}^\top \mathbf{K}_b^{-1} \mathbf{1}} - \frac{k_0^{-2}}{(\mathbf{1}^\top \mathbf{K}_b^{-1} \mathbf{1})^2} + \frac{k_0^{-4}}{(\mathbf{1}^\top \mathbf{K}_b^{-1} \mathbf{1})^3} + O(k_0^{-6}) \quad (18)$$

so that

$$\begin{aligned} m_n[f](\mathbf{x}) &= \frac{\mathbf{1}^\top \mathbf{K}_b^{-1} f(X_n)}{\mathbf{1}^\top \mathbf{K}_b^{-1} \mathbf{1}} + \mathbf{k}_b(\mathbf{x})^\top \mathbf{K}_b^{-1} \left\{ f(X_n) - \left( \frac{\mathbf{1}^\top \mathbf{K}_b^{-1} f(X_n)}{\mathbf{1}^\top \mathbf{K}_b^{-1} \mathbf{1}} \right) \mathbf{1} \right\} + O(k_0^{-2}), \\ k_n[f](\mathbf{x}, \mathbf{x}') &= \sigma^2 \left\{ k_b(\mathbf{x}, \mathbf{x}') - \mathbf{k}_b(\mathbf{x})^\top \mathbf{K}_b^{-1} \mathbf{k}_b(\mathbf{x}') + \frac{[\mathbf{k}_b(\mathbf{x})^\top \mathbf{K}_b^{-1} \mathbf{1} - 1][\mathbf{k}_b(\mathbf{x}')^\top \mathbf{K}_b^{-1} \mathbf{1} - 1]^\top}{\mathbf{1}^\top \mathbf{K}_b^{-1} \mathbf{1}} \right\} \\ &\quad + O(k_0^{-2}), \end{aligned}$$

which gives the stated limiting result.

### B.3 Technical Results on Polynomial Reproduction

The proof that we present for Theorem 2 is based on local polynomial reproduction, and we aim for a result similar to Theorem 11.13 in Wendland (2004). That result, however, aims for applicability to general domains and relies on an *interior cone condition* to ensure that fill distances based on balls can be meaningfully related to the approximation task. In our case, where the domain is axis-aligned, simpler and sharper results may be obtained by performing an alternative analysis based directly on boxes instead. Furthermore, we require a result for non-isotropic kernels, while Theorem 11.13 in Wendland (2004) assumes an isotropic kernel.

Our starting point is the following fundamental result on polynomial functions and scattered data:

**Lemma 14** (Lemma 1 in Madych and Nelson (1992)). *Let  $\gamma_1 = 2$  and  $\gamma_d = 2d(1 + \gamma_{d-1})$  for  $d > 1$ . Let  $\ell \in \mathbb{N}$  with  $q \geq \gamma_d(\ell + 1)$ . Let  $\mathcal{X} = [\mathbf{a}, \mathbf{a} + \lambda \mathbf{1}]$  for some  $\mathbf{a} \in \mathbb{R}_+^d$  and  $\lambda > 0$ . Divide  $\mathcal{X}$  into  $q^d$  identical subcubes. If  $X_n \subset \mathcal{X}$  is a set of  $n \geq q^d$  points such that each subcube contains at least one of these points, then for all  $p \in \pi_\ell(\mathbb{R}^d)$ ,*

$$\|p\|_{L^\infty(\mathcal{X})} \leq e^{2d\gamma_d(\ell+1)} \|p\|_{L^\infty(X_n)}.$$

Now let  $\mathcal{X}$  be a domain and  $X_n = \{\mathbf{x}_1, \dots, \mathbf{x}_n\} \subset \mathcal{X}$ . The elementary tool that we use is the *sampling operator*

$$\begin{aligned} T_{X_n} : \pi_\ell(\mathcal{X}) &\rightarrow \mathbb{R}^n \\ p &\mapsto (p(\mathbf{x}_1), \dots, p(\mathbf{x}_n)) \end{aligned}$$

where  $\pi_\ell(\mathcal{X})$  is equipped with the norm  $\|\cdot\|_{L^\infty(\mathcal{X})}$ . The set of pointwise evaluation functionals on  $X_n$  is called a *norming set* for  $\pi_\ell(\mathcal{X})$  if the sampling operator  $T_{X_n}$  is injective into  $\mathbb{R}^n$ . For shorthand, we simply call such  $X_n$  a norming set. The terminology comes from the fact that such a  $T_{X_n}$  can be used to induce a norm on  $\pi_\ell(\mathcal{X})$  using the norm on  $\mathbb{R}^n$ . For further details on sampling operators and norming sets, see Section 4 of Mhaskar et al. (2001). For a continuous linear function  $T : U \rightarrow V$  between normed spaces  $U$  and  $V$ , we let  $\|T\|$  denote the operator norm  $\sup_{u \neq 0} \|T(u)\|_V / \|u\|_U$ . In what follows, Propositions 15 to 17 provide analogues of Theorems 3.4, 3.8, and 11.21 of Wendland (2004) that are adapted to the case of the box fill distance (as opposed to the ball fill distance) to obtain sharper constants for use in the present context.

**Proposition 15** (Properties of the sampling operator). *Let  $\mathcal{X} = [\mathbf{a}, \mathbf{a} + \lambda \mathbf{1}]$  for some  $\mathbf{a} \in \mathbb{R}_+^d$  and  $\lambda > 0$ . Let  $\ell \in \mathbb{N}$ . Suppose that  $\rho_{X_n, \mathcal{X}} \leq \lambda / (\gamma_d(\ell + 1))$ . Then  $X_n$  is a norming set and  $\|T_{X_n}^{-1}\| \leq e^{2d\gamma_d(\ell+1)}$ .*

*Proof.* If  $T_{X_n}$  is not injective then, since  $T_{X_n}$  is linear, there must be a  $0 \neq p \in \pi_\ell(\mathcal{X})$  for which  $T_{X_n}(p) = 0$ . Let  $0 \neq p \in \pi_\ell(\mathbb{R}^d)$ . Our first task is to show that  $T_{X_n}(p) \neq 0$ . Since  $\rho_{X_n, \mathcal{X}} \leq \lambda / (\gamma_d(\ell + 1))$ , the conditions of Lemma 14 are satisfied with  $q = \gamma_d(\ell + 1)$ . Thus the conclusion of Lemma 14 holds, namely that

$$\|T_{X_n}(p)\|_\infty = \|p\|_{L^\infty(X_n)} \geq e^{-2d\gamma_d(\ell+1)} \|p\|_{L^\infty(\mathcal{X})} > 0.$$

Thus  $T_{X_n}(p) \neq 0$ , showing that  $T_{X_n}$  must be injective and  $X_n$  must be a norming set. Finally, we have also shown that

$$\|T_{X_n}^{-1}\| = \sup_{p \neq 0} \frac{\|p\|_{L^\infty(\mathcal{X})}}{\|T_{X_n}(p)\|} \leq \sup_{p \neq 0} \frac{\|p\|_{L^\infty(\mathcal{X})}}{\|T_{X_n}(p)\|_\infty} \leq e^{2d\gamma_d(\ell+1)},$$

as claimed. □

Using a norming set  $X_n$ , we can establish a global form of polynomial reproduction, as stated in the next result:

**Proposition 16** (Global polynomial reproduction). *In the setting of Proposition 15, for each  $\mathbf{x} \in \mathcal{X}$  there exists  $\mathbf{u}(\mathbf{x}) \in \mathbb{R}^n$  such that*

- $p(\mathbf{x}) = \sum_{i=1}^n u_i(\mathbf{x}) p(\mathbf{x}_i)$  for all  $p \in \pi_\ell(\mathcal{X})$ ,
- $\sum_{i=1}^n |u_i(\mathbf{x})| \leq e^{2d\gamma_d(\ell+1)}$ .

*Proof.* Define a function  $f : \text{range}(T_{X_n}) \rightarrow \mathbb{R}$  by  $f(\mathbf{v}) = T_{X_n}^{-1}(\mathbf{v})(\mathbf{x})$ . From the conclusion of Proposition 15 we have  $\|f\| \leq \|T_{X_n}^{-1}\| \leq e^{2d\gamma_d(\ell+1)}$ . By the Hahn–Banach theorem,  $f$  has a norm-preserving extension  $f_{\text{ext}}$  to  $\mathbb{R}^n$ . Since  $f_{\text{ext}}$  is a linear function on  $\mathbb{R}^n$ , it can be written as  $f_{\text{ext}}(\mathbf{v}) = \langle \mathbf{v}, \mathbf{u} \rangle$  from the Riesz representation theorem where  $\|\mathbf{u}\| = \|f_{\text{ext}}\| \leq e^{2d\gamma_d(\ell+1)}$ . Then  $p(\mathbf{x}) = f(T_{X_n}(p)) = f_{\text{ext}}(T_{X_n}(p)) = \sum_{i=1}^n u_i p(\mathbf{x}_i)$ , as required. □

The application of Proposition 16 to a collection of smaller hypercubes contained in  $\mathcal{X}$  yields the following local form of polynomial reproduction that will be used to prove Theorem 2:

**Proposition 17** (Local polynomial reproduction). *Suppose that  $\mathcal{X} = [\mathbf{0}, \gamma \mathbf{1}]$ . Let  $\ell \in \mathbb{N}$  and  $0 < \lambda \leq \gamma$ . Suppose that  $\rho_{X_n, \mathcal{X}} \leq \lambda / (\gamma_d(\ell + 1))$ . Then for all  $\mathbf{x} \in \mathcal{X}$  there exist numbers  $u_i(\mathbf{x})$  with*

- $\sum_{i=1}^n u_i(\mathbf{x}) p(\mathbf{x}_i) = p(\mathbf{x})$  for all  $p \in \pi_\ell(\mathcal{X})$ ,
- $\sum_{i=1}^n |u_i(\mathbf{x})| \leq e^{2d\gamma_d(\ell+1)}$ ,
- $u_i(\mathbf{x}) = 0$  if  $\|\mathbf{x} - \mathbf{x}_i\|_\infty > \lambda$ .

*Proof.* Given  $\mathbf{x} \in \mathcal{X}$  we can find a box  $\mathcal{X}_{\mathbf{x}} := [\mathbf{a}, \mathbf{a} + \lambda \mathbf{1}] \subset \mathcal{X}$  with  $\mathbf{x} \in \mathcal{X}_{\mathbf{x}}$ . Let  $Y_n := X_n \cap \mathcal{X}_{\mathbf{x}} = \{\mathbf{y}_1, \dots, \mathbf{y}_m\}$ . The box  $\mathcal{X}_{\mathbf{x}}$  and the set  $Y_n$  satisfy the conditions of Proposition 16 and thus there exists  $\tilde{u}_i(\mathbf{x})$  such that

- $p(\mathbf{x}) = \sum_{i=1}^m \tilde{u}_i(\mathbf{x}) p(\mathbf{y}_i)$  for all  $p \in \pi_\ell(\mathbb{R}^d)$ ,
- $\sum_{i=1}^m |\tilde{u}_i(\mathbf{x})| \leq e^{2d\gamma_d(\ell+1)}$ .

From here we define  $u_i(\mathbf{x}) = \tilde{u}_j(\mathbf{x})$  if  $\mathbf{x}_i = \mathbf{y}_j$ , otherwise we define  $u_i(\mathbf{x}) = 0$ , ensuring that  $u_i(\mathbf{x}) = 0$  if  $\|\mathbf{x} - \mathbf{x}_i\|_\infty > \lambda$ .  $\square$

## B.4 Proof of Theorem 2

This section contains the proof of Theorem 2. Before we begin, it is useful to recall that  $\mathcal{H}_k(\mathcal{X})$  is endowed with the semi-norm  $|f|_{\mathcal{H}_k(\mathcal{X})}$  which can be computed using either of the equivalent formulations  $\|\mathbf{x} \mapsto f(\mathbf{x}) - f(\mathbf{0})\|_{\mathcal{H}_{k_b}(\mathcal{X})}$  or  $\|\mathbf{x} \mapsto (f(\mathbf{x}) - f(\mathbf{0})) / b(\mathbf{x})\|_{\mathcal{H}_{k_e}(\mathcal{X})}$  (Paulsen and Raghupathi, 2016, Theorem 5.16); here the latter formulation will be used. Let  $\mathcal{S}(X_n)$  denote the set of linear functionals of the form  $\mathbf{s}[f] = \mathbf{w}^\top f(X_n)$  whose weights are normalised such that  $\mathbf{1}^\top \mathbf{w} = 1$ .

**Proposition 18.** *The extrapolated mean estimator  $\mathbf{s}[f] = m_n[f](\mathbf{0})$  from (6) minimises the worst case error*

$$\text{wce}(\mathbf{s}) := \sup \{ |f(\mathbf{0}) - \mathbf{s}[f]| : |f|_{\mathcal{H}_k(\mathcal{X})} \leq 1 \}$$

*among all estimators  $\mathbf{s} \in \mathcal{S}(X_n)$ .*

*Proof.* Consider a general element  $\mathbf{s} \in \mathcal{S}(X_n)$ , which has the form  $\mathbf{s}[f] = \mathbf{w}^\top f(X_n)$  where  $\mathbf{1}^\top \mathbf{w} = 1$ . Since the weights  $\mathbf{w}$  are normalised,  $\mathbf{s}$  is exact on constant functions, and thus  $f(\mathbf{0}) - \mathbf{s}[f] = \mathbf{s}[f(\mathbf{0}) - f]$  where  $f(\mathbf{0}) - f \in \mathcal{H}_{k_b}(\mathcal{X})$ . It follows that

$$\text{wce}(\mathbf{s}) = \sup \{ |\mathbf{s}[f]| : \|f\|_{\mathcal{H}_{k_b}(\mathcal{X})} \leq 1 \}.$$

It has been assumed that the elements of  $X_n$  are distinct. The Riesz representer of the error functional  $f \mapsto f(\mathbf{0}) - \mathbf{w}^\top f(X_n)$  is  $k_b(\mathbf{0}, \cdot) - \mathbf{w}^\top \mathbf{k}_b(\cdot)$  and, since  $\text{wce}(\mathbf{s})$  is the operator norm of the error functional and Hilbert spaces are self-dual, we have that

$$\begin{aligned} \text{wce}(\mathbf{s})^2 &= \left\| k_b(\mathbf{0}, \cdot) - \mathbf{w}^\top \mathbf{k}_b(\cdot) \right\|_{\mathcal{H}_{k_b}(\mathcal{X})}^2 = k_b(\mathbf{0}, \mathbf{0}) - 2\mathbf{w}^\top \mathbf{k}_b(\mathbf{0}) + \mathbf{w}^\top \mathbf{K}_b \mathbf{w} \\ &= \mathbf{w}^\top \mathbf{K}_b \mathbf{w} \end{aligned} \quad (19)$$

where the final equality follows since  $k_b(\mathbf{0}, \mathbf{x}) = b(\mathbf{0})b(\mathbf{x})k_e(\mathbf{0}, \mathbf{x}) = 0$  for all  $\mathbf{x} \in \mathcal{X}$ . This leaves a quadratic form in  $\mathbf{w}$  and we seek the minimum subject to  $\mathbf{1}^\top \mathbf{w} = 1$ . If we consider the Lagrangian

$$\mathcal{L}(\mathbf{w}, \lambda) = \mathbf{w}^\top \mathbf{K}_b \mathbf{w} + \lambda(\mathbf{1}^\top \mathbf{w} - 1)$$

then we have a critical point when  $\partial_{\mathbf{w}} \mathcal{L} = 2\mathbf{K}_b \mathbf{w} + \lambda \mathbf{1} = 0$ , so that  $\mathbf{w} = -\frac{\lambda}{2} \mathbf{K}_b^{-1} \mathbf{1}$ . Enforcing the normalisation constraint leads to  $\mathbf{w} = \mathbf{K}_b^{-1} \mathbf{1} / (\mathbf{1}^\top \mathbf{K}_b^{-1} \mathbf{1})$ , which means that  $\mathbf{s}[f] = \mathbf{w}^\top f(X_n) = m_n[f](\mathbf{0})$ , as claimed.  $\square$

The proof of Theorem 2 below employs the *multi-index* notation, meaning that for  $\boldsymbol{\beta} \in \mathbb{N}_0^d$  we let  $|\boldsymbol{\beta}| := \beta_1 + \dots + \beta_d$ ,  $\boldsymbol{\beta}! := \beta_1! \dots \beta_d!$ , and  $\mathbf{z}^\boldsymbol{\beta} := z_1^{\beta_1} \dots z_d^{\beta_d}$  for  $\mathbf{z} \in \mathbb{R}^d$ .

*Proof of Theorem 2.* Assume without loss of generality that  $|f|_{\mathcal{H}_k(\mathcal{X})} \neq 0$ , since otherwise  $m_n^h[f] = 0$  is trivially exact. Let  $\mathbf{x}_i^h = h\mathbf{x}_i$  and  $k_b(\mathbf{x}, \mathbf{y}) = b(\mathbf{x})b(\mathbf{y})k_e(\mathbf{x}, \mathbf{y})$  in shorthand. Introduce the positive semi-definite quadratic form

$$Q(\mathbf{u}) = \sum_{i=1}^n \sum_{j=1}^n u_i u_j k_b(\mathbf{x}_i^h, \mathbf{x}_j^h) \quad (20)$$

and note from Proposition 18 that

$$\frac{|f(\mathbf{0}) - m_n^h[f](\mathbf{0})|}{|f|_{\mathcal{H}(k)}} \leq \text{wce}(m_n^h[f]) = \min \left\{ Q(\mathbf{u})^{1/2} : \mathbf{u} \in \mathbb{R}^n, \sum_{i=1}^n u_i = 1 \right\}. \quad (21)$$

Thus we can bound the relative error by the square root of  $Q(\mathbf{u})$  for any choice of  $\mathbf{u} \in \mathbb{R}^n$  for which  $\sum_{i=1}^n u_i = 1$ . Our choice of  $\mathbf{u}$  will be based on polynomial reproduction, as described next.

From Taylor's theorem, since  $k_e(\mathbf{x}, \cdot) \in C^{2s}(\mathcal{X}_h)$ ,

$$k_e(\mathbf{x}, \mathbf{y}) = \sum_{|\boldsymbol{\beta}| < 2s} \frac{\partial_{\mathbf{z}}^\boldsymbol{\beta} k_e(\mathbf{x}, \mathbf{z})|_{\mathbf{z}=\mathbf{x}}}{\boldsymbol{\beta}!} (\mathbf{y} - \mathbf{x})^\boldsymbol{\beta} + R(\mathbf{x}, \mathbf{y}), \quad |R(\mathbf{x}, \mathbf{y})| \leq C_{\mathbf{x}}^{(2s)} \|\mathbf{x} - \mathbf{y}\|^{2s} \quad (22)$$

for all  $\mathbf{x}, \mathbf{y} \in \mathcal{X}_h$ , where the constants  $C_{\mathbf{x}}^{(2s)} := ((2s)!)^{-1} \sup_{\mathbf{z} \in \mathcal{X}_h} \sum_{|\boldsymbol{\beta}|=2s} \partial_{\mathbf{z}}^\boldsymbol{\beta} k_e(\mathbf{x}, \mathbf{z})$  are uniformly bounded by  $C_k^{(2s)} := \sup_{\mathbf{x} \in \mathcal{X}} C_{\mathbf{x}}^{(2s)}$  since  $\mathcal{X}$  is compact. Plugging this into (20) gives that

$$Q(\mathbf{u}) = \sum_{i=1}^n u_i b(\mathbf{x}_i^h) \sum_{j=1}^n u_j b(\mathbf{x}_j^h) \left( \sum_{|\boldsymbol{\beta}| < 2s} \frac{\partial_{\mathbf{z}}^\boldsymbol{\beta} k_e(\mathbf{x}_i^h, \mathbf{z})|_{\mathbf{z}=\mathbf{x}_i^h}}{\boldsymbol{\beta}!} (\mathbf{x}_j^h - \mathbf{x}_i^h)^\boldsymbol{\beta} + R(\mathbf{x}_i^h, \mathbf{x}_j^h) \right).$$

Since  $b(\mathbf{x}_j^h)(\mathbf{x}_j^h - \mathbf{x}_i^h)^\beta$  is a polynomial in  $\mathbf{x}_j^h$  of total degree at most  $r + |\beta|$  and  $|\beta| < 2s$ , we aim to pick a vector  $\mathbf{u}$  for which local (at  $\mathbf{0}$ ) polynomial reproduction on  $X_n^h$  occurs up to polynomials of total order  $\ell := r + (2s - 1)$ . Set  $\lambda := \gamma_d(\ell + 1)\rho_{X_n^h, \mathcal{X}_h} = \gamma_d(\ell + 1)h\rho_{X_n, \mathcal{X}}$ , so that our assumption on the box fill distance implies  $0 < \lambda \leq h$ , and trivially  $\rho_{X_n^h, \mathcal{X}_h} \leq \lambda/(\gamma_d(\ell + 1))$ . Thus the conditions of Proposition 17 are satisfied, and there exists  $\mathbf{u} \in \mathbb{R}^n$  such that

- $\sum_{i=1}^n u_i p(\mathbf{x}_i^h) = p(\mathbf{0})$  for all  $p \in \pi_\ell(\mathcal{X}_h)$ ,
- $\sum_{i=1}^n |u_i| \leq e^{2d\gamma_d(\ell+1)}$ ,
- $u_i = 0$  if  $\mathbf{x}_i^h \notin [\mathbf{0}, \lambda\mathbf{1}]$ .

For this choice of  $\mathbf{u}$  it follows from the local polynomial reproduction property that, for  $|\beta| < 2s$ ,

$$\sum_{j=1}^n u_j b(\mathbf{x}_j^h)(\mathbf{x}_j^h - \mathbf{x}_i^h)^\beta = b(\mathbf{x})(\mathbf{x} - \mathbf{x}_i^h)^\beta \Big|_{\mathbf{x}=\mathbf{0}} = b(\mathbf{0})(-\mathbf{x}_i^h)^\beta = \mathbf{0}$$

since  $b(\mathbf{0}) = 0$ , and thus, recalling that  $u_i = 0$  whenever  $\mathbf{x}_i^h \notin [\mathbf{0}, \lambda\mathbf{1}]$ ,

$$Q(\mathbf{u}) = \sum_{i=1}^n u_i b(\mathbf{x}_i^h) \sum_{j=1}^n u_j b(\mathbf{x}_j^h) R(\mathbf{x}_i^h, \mathbf{x}_j^h) \leq \|\mathbf{u}\|_1^2 \|b\|_{L^\infty(\mathcal{X}_h)}^2 \sup_{\mathbf{x}, \mathbf{y} \in [\mathbf{0}, \gamma\mathbf{1}]} |R(\mathbf{x}, \mathbf{y})|,$$

where by construction  $\|\mathbf{u}\|_1 \leq e^{2d\gamma_d(\ell+1)}$ . The final term can be bounded using the error estimate in (22):

$$\begin{aligned} \sup_{\mathbf{x}, \mathbf{y} \in [\mathbf{0}, \gamma\mathbf{1}]} |R(\mathbf{x}, \mathbf{y})| &\leq \sup_{\mathbf{x} \in [\mathbf{0}, \gamma\mathbf{1}]} C_{\mathbf{x}}^{(2s)} \times \|\mathbf{0} - \lambda\mathbf{1}\|^{2s} \leq C_k^{(2s)} \frac{d^s}{(2s)!} \lambda^{2s} \\ &= C_k^{(2s)} \frac{d^s}{(2s)!} (\gamma_d(\ell + 1)h\rho_{X_n, \mathcal{X}})^{2s}, \end{aligned}$$

leading to the claimed overall bound  $\text{wce}(m_n^h[f]) \leq C_{r,s} h^s \rho_{X_n, \mathcal{X}}^s \|b\|_{L^\infty(\mathcal{X}_h)}$  on the relative error, where  $C_{r,s} := (C_k^{(2s)})^{1/2} d^{s/2} e^{2d\gamma_d(\ell+1)} \gamma_d^s (\ell + 1)^s / \sqrt{(2s)!}$ .  $\square$

## B.5 Proof of Theorem 4

*Proof of Theorem 4.* The assumption on the growth of the derivatives of  $k_e$  implies that  $C_k^{(2s)} \leq C_k^{2s}$  for the assumed constant  $C_k$ , and we employ this bound throughout. Now, to more easily track the  $s$ -dependent constants in the bound of Theorem 2 we employ a simpler upper bound

$$C_{r,s} h^s \rho_{X_n, \mathcal{X}}^s = \frac{C_k^s d^{s/2} e^{2d\gamma_d(r+2s)} \gamma_d^s (r+2s)^s}{\sqrt{(2s)!}} h^s \rho_{X_n, \mathcal{X}}^s \leq e^{2d\gamma_d r} \left( \frac{C_k d^{1/2} e^{4d\gamma_d+1} h}{2s} \right)^s \quad (23)$$



which holds whenever  $\rho_{X_n, \mathcal{X}} \leq 1/(\gamma_d(r+2s))$ , and where we used the elementary fact  $1/\sqrt{(2s)!} \leq (e/(2s))^s$  to obtain this simpler bound.

The idea of this proof is to pick a particular value of  $s \in \mathbb{N}_0$  that will be  $\rho_{X_n, \mathcal{X}}$ -dependent. For (23) to hold we require  $\rho_{X_n, \mathcal{X}} \leq 1/(\gamma_d(r+2s))$ , and the largest such  $s$  for which this requirement is satisfied is

$$s^* := \left\lfloor -\frac{r}{2} + \frac{1}{2\gamma_d\rho_{X_n, \mathcal{X}}} \right\rfloor. \quad (24)$$

The assumption  $\rho_{X_n, \mathcal{X}} \leq 1/(2\gamma_d(r+1))$  implies  $s^* \geq 1/(4\gamma_d\rho_{X_n, \mathcal{X}}) \geq 0$ , so  $s$  is well-defined as an element of  $\mathbb{N}_0$ . Further, the assumption  $\rho_{X_n, \mathcal{X}} \leq 1/(2d^{1/2}\gamma_d e^{4d\gamma_d+1})$  implies  $t \mapsto [(\frac{1}{2}d^{1/2}e^{4d\gamma_d+1}h)/t]^t$  is decreasing on  $t \in [1/(4\gamma_d\rho_{X_n, \mathcal{X}}), \infty)$  for any  $h \in (0, 1]$ . Thus we can replace  $s$  by  $1/(4\gamma_d\rho_{X_n, \mathcal{X}})$  in (23) to obtain the upper bound

$$C_{r,s}h^s\rho_{X_n, \mathcal{X}}^s \leq e^{2d\gamma_d r} \left( \frac{\frac{1}{2}C_k d^{1/2} e^{4d\gamma_d+1} h}{1/(4\gamma_d\rho_{X_n, \mathcal{X}})} \right)^{1/(4\gamma_d\rho_{X_n, \mathcal{X}})} = C_{n,r,s} h^{\frac{1}{4\gamma_d\rho_{X_n, \mathcal{X}}}}$$

where  $C_{n,r,s} := (2C_k d^{1/2} \gamma_d e^{4d\gamma_d+1} \rho_{X_n, \mathcal{X}})^{1/(4\gamma_d\rho_{X_n, \mathcal{X}})}$  is a  $h$ -independent constant. The assumptions we made above on the box fill distance are satisfied when  $\rho_{X_n, \mathcal{X}} \leq \min\{1/(2\gamma_d(r+1)), 1/(2d^{1/2}\gamma_d e^{4d\gamma_d+1})\}$ .  $\square$

## B.6 Verifying the Assumptions for Example 5

The aim of this appendix is to verify that the function  $\psi(x) = \sin(10x) + 1_{x>0}x^{s+4}$  satisfies  $\psi(x) = c_0 + c_1x + c_2x^2 + c_3(x)x^3$  for some  $c_0, c_1, c_2 \in \mathbb{R}$  and  $c_3 \in H^{s+1}(\mathcal{O})$  where  $\mathcal{O} = (-\delta, \delta)$ ,  $\delta > 0$ , is an open neighbourhood of 0 and we recall that  $H^{s+1}(\mathcal{O})$  is the Sobolev space of  $s+1$  times weakly differentiable functions on  $\mathcal{O}$ ; see Appendix A. It then follows from Appendix A that  $x \mapsto c_3(x)$  and  $x \mapsto c_3(-x)$  are elements of  $\mathcal{H}_{k_e}(\mathcal{X})$  whenever  $k_e$  is either the Matérn or Wendland kernel with smoothness  $s$  and  $\mathcal{X} = [0, \delta)$ , since these kernels reproduce (up to an equivalent norm)  $H^{s+1}(\mathcal{X})$  in dimension  $d = 1$ .

From linearity, it suffices to establish this fact separately for  $\psi_1(x) := \sin(10x)$  and  $\psi_2(x) := 1_{x>0}x^{s+4}$ . For the first term, since the trigonometric functions are real-analytic, we have a convergent power series  $\psi_1(x) = \sum_{i=0}^{\infty} \tilde{c}_i x^i$  for  $x \in [-\epsilon, \epsilon]$  for some  $\epsilon > 0$ . Thus  $\psi_1(x) = \tilde{c}_0 + \tilde{c}_1x + \tilde{c}_2x^2 + c_3(x)x^3$  with  $c_3(x) = \sum_{i=3}^{\infty} \tilde{c}_i x^{i-3}$ , and our task is to show that this latter series is convergent in a neighbourhood of  $x = 0$ . To this end, we restrict attention to  $x \in [-\epsilon/2, \epsilon/2]$ , and then use the ratio test

$$\frac{|\tilde{c}_i x^{i-3}|}{|\tilde{c}_i \epsilon^i|} = \frac{1}{|x|^3} \left| \frac{x}{\epsilon} \right|^i \leq \frac{1}{|x|^3} \frac{1}{2^i} \rightarrow 0 \quad \text{as } i \rightarrow \infty$$

to deduce absolute convergence of the series, as required. For the second term, we take  $c_0 = c_1 = c_2 = 0$ , so that  $\psi_2(x) = c_3(x)x^3$  where  $c_3(x) = 1_{x>0}x^{s+1}$ , observing that  $c_3$  has an  $(s+1)$ -order weak derivative  $c_3^{(s+1)}(x)$  taking the value 0 on  $x \leq 0$  and  $(s+1)!$  on  $x > 0$ , so that  $c_3 \in H^{s+1}(\mathcal{O})$ .

## B.7 Proof of Proposition 6 and Corollary 7

*Proof of Proposition 6.* Our assumption implies  $(e_n)_{n \in \mathbb{N}}$  is Cauchy and thus this sequence converges to a limit, denoted  $e_\infty \in \mathbb{R}$ . Let  $\varphi : [0, \infty) \rightarrow [0, 1]$  be a smooth function with  $\varphi(0) = 0$ ,  $\varphi = 1$  on  $[1, \infty)$ , and derivatives uniformly bounded. Let

$$e(\mathbf{x}) := \begin{cases} e_\infty & \text{if } \mathbf{x} = \mathbf{0}, \\ e_{n+1} + (e_n - e_{n+1}) \prod_{i=1}^d \varphi\left(\frac{x_i - \mathbf{x}_{n+1,i}}{\mathbf{x}_{n,i} - \mathbf{x}_{n+1,i}}\right) & \text{if } \mathbf{x} \in [\mathbf{0}, \mathbf{x}_n] \setminus [\mathbf{0}, \mathbf{x}_n], \\ e_1 & \text{if } \mathbf{x} \notin [\mathbf{0}, \mathbf{x}_1] \end{cases}$$

so that  $e(\mathbf{x}_n) = e_n$  and  $e(\mathbf{0}) = e_\infty$ . Now set  $f(\mathbf{x}) = y_\infty + b(\mathbf{x})e(\mathbf{x})$ . To establish  $|f|_{\mathcal{H}_k(\mathcal{X})} < \infty$  it suffices to establish that  $\lim_{\mathbf{x} \rightarrow \mathbf{0}} \partial^\beta e(\mathbf{x})$  exists and is finite for all  $|\beta| = p$ , since then we will have  $e \in C^p(\mathcal{X}) \subset \mathcal{H}(k_e)$ . This is indeed the case, since on  $[\mathbf{0}, \mathbf{x}_n] \setminus [\mathbf{0}, \mathbf{x}_n]$  we have that

$$\partial^\beta e(\mathbf{x}) = (e_n - e_{n+1}) \prod_{i=1}^d \varphi^{(\beta_i)}\left(\frac{x_i - \mathbf{x}_{n+1,i}}{\mathbf{x}_{n,i} - \mathbf{x}_{n+1,i}}\right) \frac{1}{(\mathbf{x}_{n,i} - \mathbf{x}_{n+1,i})^{\beta_i}}.$$

where the  $\varphi^{(\beta_i)}$  terms are uniformly bounded and the remaining terms vanish since

$$|e_n - e_{n+1}| \prod_{i=1}^d \frac{1}{(\mathbf{x}_{n,i} - \mathbf{x}_{n+1,i})^{\beta_i}} \leq \frac{|e_n - e_{n+1}|}{\min(\mathbf{x}_n - \mathbf{x}_{n+1})^p}$$

where  $p = \beta_1 + \dots + \beta_d$ , and this final bound was assumed to vanish.  $\square$

*Proof of Corollary 7.* The renormalised error is  $e_n = C_1 + C_2 x_n^{p+1} + O(x_n^{p+2})$ , so that

$$\frac{e_n - e_{n+1}}{(x_n - x_{n+1})^p} = C_2 \frac{(x_n^{p+1} - x_{n+1}^{p+1})}{(x_n - x_{n+1})^p} + \frac{O(x_n^{p+2}) + O(x_{n+1}^{p+2})}{(x_n - x_{n+1})^p} \rightarrow 0.$$

Our assumptions on the sequence  $(x_n)_{n \in \mathbb{N}}$  imply that both terms vanish in the  $n \rightarrow \infty$  limit.  $\square$

## B.8 Proof of Proposition 9

First we establish the correctness of the algebraic identity (8) given in the main text. Again, it is useful to recall that  $\mathcal{H}_k(\mathcal{X})$  is endowed with the semi-norm  $|f|_{\mathcal{H}_k(\mathcal{X})}$  which can be computed using either of the equivalent formulations  $\|\mathbf{x} \mapsto f(\mathbf{x}) - f(\mathbf{0})\|_{\mathcal{H}_{k_b}(\mathcal{X})}$  or  $\|\mathbf{x} \mapsto (f(\mathbf{x}) - f(\mathbf{0}))/b(\mathbf{x})\|_{\mathcal{H}_{k_e}(\mathcal{X})}$  (Paulsen and Raghupathi, 2016, Theorem 5.16); here the latter formulation will be used.

**Proposition 19.** *The estimator  $\sigma_n^2[f] := \frac{1}{n} |m_n[f]|_{\mathcal{H}_k(\mathcal{X})}^2$  has the explicit form*

$$\sigma_n^2[f] = \frac{1}{n} \left[ f(X_n)^\top \mathbf{K}_b^{-1} f(X_n) - \frac{(\mathbf{1}^\top \mathbf{K}_b^{-1} f(X_n))^2}{\mathbf{1}^\top \mathbf{K}_b^{-1} \mathbf{1}} \right]$$

given in (8) of the main text.

*Proof.* Let  $\bar{m}_n[f] = m_n[f] - m_n[f](\mathbf{0})$ . From direct calculation,

$$\begin{aligned}
|m_n[f]|_{\mathcal{H}_k(\mathcal{X})}^2 &= \|\bar{m}_n[f]\|_{\mathcal{H}_{k_b}(\mathcal{X})}^2 \\
&= \left\| \mathbf{K}_b(\cdot)^\top \mathbf{K}_b^{-1} \left\{ f(X_n) - \left( \frac{\mathbf{1}^\top \mathbf{K}_b^{-1} f(X_n)}{\mathbf{1}^\top \mathbf{K}_b^{-1} \mathbf{1}} \right) \mathbf{1} \right\} \right\|_{\mathcal{H}_{k_b}(\mathcal{X})}^2 \\
&= \left\{ f(X_n) - \left( \frac{\mathbf{1}^\top \mathbf{K}_b^{-1} f(X_n)}{\mathbf{1}^\top \mathbf{K}_b^{-1} \mathbf{1}} \right) \mathbf{1} \right\}^\top \mathbf{K}_b^{-1} \left\{ f(X_n) - \left( \frac{\mathbf{1}^\top \mathbf{K}_b^{-1} f(X_n)}{\mathbf{1}^\top \mathbf{K}_b^{-1} \mathbf{1}} \right) \mathbf{1} \right\} \\
&= f(X_n)^\top \mathbf{K}_b^{-1} f(X_n) - \frac{(\mathbf{1}^\top \mathbf{K}_b^{-1} f(X_n))^2}{\mathbf{1}^\top \mathbf{K}_b^{-1} \mathbf{1}},
\end{aligned}$$

which completes the proof.  $\square$

Next we present a general result, which forms the crux of the argument in our proof of Proposition 9:

**Proposition 20.** *Assume that  $f \in \mathcal{H}_k(\mathcal{X})$ . Then*

$$\frac{|f(\mathbf{0}) - m_n[f](\mathbf{0})|}{\sqrt{k_n[f](\mathbf{0}, \mathbf{0})}} \leq \frac{|f|_{\mathcal{H}_k(\mathcal{X})}}{\sigma_n[f]}.$$

*Proof.* From (19) in the the proof of Proposition 18, we have  $\text{wce}(\mathbf{s})^2 = \mathbf{w}^\top \mathbf{K}_b \mathbf{w}$  for any algorithm  $\mathbf{s}[f] = \mathbf{w}^\top f(X_n)$  with  $\mathbf{1}^\top \mathbf{w} = 1$ . In particular, we can consider the algorithm  $\mathbf{s}[f] = m_n[f](\mathbf{0})$ , which has  $\mathbf{w} = \mathbf{K}_b^{-1} \mathbf{1} / (\mathbf{1}^\top \mathbf{K}_b^{-1} \mathbf{1})$ , to see that

$$\text{wce}(\mathbf{s})^2 = \left( \frac{\mathbf{K}_b^{-1} \mathbf{1}}{\mathbf{1}^\top \mathbf{K}_b^{-1} \mathbf{1}} \right)^\top \mathbf{K}_b \left( \frac{\mathbf{K}_b^{-1} \mathbf{1}}{\mathbf{1}^\top \mathbf{K}_b^{-1} \mathbf{1}} \right) = \frac{1}{\mathbf{1}^\top \mathbf{K}_b^{-1} \mathbf{1}} = \frac{k_n[f](\mathbf{0}, \mathbf{0})}{\sigma_n^2[f]}.$$

This implies that

$$\frac{|f(\mathbf{0}) - m_n[f](\mathbf{0})|}{\sqrt{k_n[f](\mathbf{0}, \mathbf{0})}} \leq \frac{\text{wce}(\mathbf{s}) |f|_{\mathcal{H}_k(\mathcal{X})}}{\sqrt{k_n[f](\mathbf{0}, \mathbf{0})}} \leq \frac{|f|_{\mathcal{H}_k(\mathcal{X})}}{\sigma_n[f]},$$

from which the result is established.  $\square$

*Proof of Proposition 9.* For  $f \in \mathcal{H}_k(\mathcal{X})$  we have the decomposition  $f(\mathbf{x}) = f(\mathbf{0}) + \bar{f}(\mathbf{x})$  with  $\bar{f} \in \mathcal{H}_{k_b}(\mathcal{X})$ , and  $|f|_{\mathcal{H}_k(\mathcal{X})} = \|\bar{f}\|_{\mathcal{H}_{k_b}(\mathcal{X})}$ . From Proposition 20 and  $\sigma_n^2[f] = \frac{1}{n} |m_n[f]|_{\mathcal{H}_k(\mathcal{X})}^2$ , it follows that

$$\frac{|f(\mathbf{0}) - m_n^h[f](\mathbf{0})|}{\sqrt{k_n^h[f](\mathbf{0}, \mathbf{0})}} \leq \frac{n |f|_{\mathcal{H}_k(\mathcal{X})}}{|m_n^h[f]|_{\mathcal{H}_k(\mathcal{X})}} = \frac{n \|\bar{f}\|_{\mathcal{H}_{k_b}(\mathcal{X})}}{\|\bar{m}_n^h[f]\|_{\mathcal{H}_{k_b}(\mathcal{X})}},$$

where similarly we have decomposed  $m_n^h[f](\mathbf{x}) = m_n^h[f](\mathbf{0}) + \bar{m}_n^h[f](\mathbf{x})$ . Since  $\bar{f}$  and  $\bar{m}_n^h[f]$  are elements of  $\mathcal{H}_{k_b}(\mathcal{X})$  and  $k_b(\mathbf{x}, \mathbf{x}') = b(\mathbf{x})b(\mathbf{x}')k_e(\mathbf{x}, \mathbf{x}')$ , we may write

$$\bar{f}(\mathbf{x}) = b(\mathbf{x})e(\mathbf{x}) \quad \text{and} \quad \bar{m}_n^h[f](\mathbf{x}) = b(\mathbf{x})\tilde{e}_n(\mathbf{x})$$

for certain  $e, \tilde{e}_h \in \mathcal{H}_{k_e}(\mathcal{X})$ , with  $\|\bar{f}\|_{\mathcal{H}_{k_b}(\mathcal{X})} = \|e\|_{\mathcal{H}_{k_e}(\mathcal{X})}$  and  $\|\bar{m}_n^h[f]\|_{\mathcal{H}_{k_b}(\mathcal{X})} = \|\tilde{e}_h\|_{\mathcal{H}_{k_e}(\mathcal{X})}$ . Therefore

$$\frac{|f(\mathbf{0}) - m_n^h[f](\mathbf{0})|}{\sqrt{k_n^h[f](\mathbf{0}, \mathbf{0})}} \leq \frac{n\|e\|_{\mathcal{H}_{k_e}(\mathcal{X})}}{\|\tilde{e}_h\|_{\mathcal{H}_{k_e}(\mathcal{X})}}. \quad (25)$$

By construction,  $m_n^h[f](h\mathbf{x}_i) = f(h\mathbf{x}_i)$  for  $i = 1, \dots, n$ . Because  $f(\mathbf{x}) = f(\mathbf{0}) + b(\mathbf{x})e(\mathbf{x})$ , the function  $\tilde{e}_h$  satisfies

$$\tilde{e}_h(h\mathbf{x}_i) = e(h\mathbf{x}_i) + b(h\mathbf{x}_i)^{-1}[f(\mathbf{0}) - m_n^h[f](\mathbf{0})]$$

for each  $i = 1, \dots, n$ . The assumptions of Theorem 2 with  $s = 1$  are satisfied, and thus

$$b(h\mathbf{x}_i)^{-1}|f(\mathbf{0}) - m_n^h[f](\mathbf{0})| \leq C_{r,1} h \rho_{X_n, \mathcal{X}} \frac{\|b\|_{L^\infty(\mathcal{X}_h)}}{b(h\mathbf{x}_i)} |f|_{\mathcal{H}_k(\mathcal{X})} \rightarrow 0$$

as  $h \rightarrow 0$  since,  $b$  being a polynomial,  $\lim_{h \rightarrow 0} \|b\|_{L^\infty(\mathcal{X}_h)} b(h\mathbf{x}_i)^{-1} < \infty$ . The continuity of  $e$ , which follows from  $e \in \mathcal{H}_{k_e}(\mathcal{X})$  and the continuity of  $k_e$ , then implies that  $\tilde{e}_h(h\mathbf{x}_i) \rightarrow e(\mathbf{0})$  as  $h \rightarrow 0$ . Let  $c \in \mathbb{R}$ . The function  $g(\mathbf{x}) := c k_e(\mathbf{x}, \mathbf{x}') k_e(\mathbf{x}', \mathbf{x}')^{-1}$  has minimal norm among all functions in  $\mathcal{H}_{k_e}(\mathcal{X})$  that equal  $c$  at  $\mathbf{x}'$  (Paulsen and Raghupathi, 2016, Corollary 3.5). By the reproducing property  $\langle k_e(\cdot, \mathbf{x}_1), k_e(\cdot, \mathbf{x}_2) \rangle_{\mathcal{H}_{k_e}(\mathcal{X})} = k_e(\mathbf{x}_1, \mathbf{x}_2)$  in the RKHS inner product, from which it follows that the norm of this function is

$$\|g\|_{\mathcal{H}_{k_e}(\mathcal{X})} = \langle g, g \rangle_{\mathcal{H}_{k_e}(\mathcal{X})}^{1/2} = |c| k_e(\mathbf{x}', \mathbf{x}')^{1/2}.$$

Consequently, setting  $\mathbf{x}' = h\mathbf{x}_1$  and  $c = \tilde{e}_h(h\mathbf{x}_1)$  gives

$$\|\tilde{e}_h\|_{\mathcal{H}_{k_e}(\mathcal{X})} \geq |\tilde{e}_h(h\mathbf{x}_1)| k_e(h\mathbf{x}_1, h\mathbf{x}_1)^{-1/2} \rightarrow |e(\mathbf{0})| k_e(\mathbf{0}, \mathbf{0})^{-1/2}.$$

Using this bound in (25) then shows that the ratio on the left-hand side is bounded as  $h \rightarrow 0$ , since we have assumed  $e(\mathbf{0}) \neq 0$ .  $\square$

## B.9 Proof of Proposition 12

*Proof of Proposition 12.* Recall that the estimator  $\mathbf{r}_n^h[f]$  is any maximiser of

$$\mathcal{L}_n^h(\mathbf{r}) = - \underbrace{\left\{ f(X_n^h)^\top \mathbf{K}_{b_r, h}^{-1} f(X_n^h) - \frac{(\mathbf{1}^\top \mathbf{K}_{b_r, h}^{-1} f(X_n^h))^2}{\mathbf{1}^\top \mathbf{K}_{b_r, h}^{-1} \mathbf{1}} \right\}}_{=: Q_n^h(f, \mathbf{r})} - \log \det \mathbf{K}_{b_r, h}.$$

Maximising  $\mathcal{L}_n^h(\mathbf{r})$  is equivalent to maximising

$$\mathcal{J}_n^h(\mathbf{r}) = \mathcal{L}_n^h(\mathbf{r}) - \mathcal{L}_n^h(\mathbf{r}_0).$$

Let  $\bar{f}(\mathbf{x}) := f(\mathbf{x}) - f(\mathbf{0})$ . By assumption,  $\bar{f}$  is an element of the RKHS of the covariance function  $k_{b_{r_0}}$ . According to Proposition 19,  $Q_n^h(f, \mathbf{r}) = |m_n^h[f]|_{\mathcal{H}_k(\mathcal{X})}^2 \geq 0$ . Also from

Proposition 19 and the minimal norm characterisation of the interpolant, we obtain the  $h$ -independent bound  $Q_n^h(f, \mathbf{r}_0) \leq \|\bar{f}\|_{\mathcal{H}_{k_{b_{\mathbf{r}_0}}}}^2(\mathcal{X})$ . Therefore

$$\begin{aligned} \mathcal{J}_n^h(\mathbf{r}) &= Q_n^h(f, \mathbf{r}_0) + \log \det \mathbf{K}_{b_{\mathbf{r}_0}, h} - Q_n^h(f, \mathbf{r}) - \log \det \mathbf{K}_{b_{\mathbf{r}}, h} \\ &\leq \log \det \mathbf{K}_{b_{\mathbf{r}_0}, h} - \log \det \mathbf{K}_{b_{\mathbf{r}}, h} + \|\bar{f}\|_{\mathcal{H}_{k_{b_{\mathbf{r}_0}}}}^2(\mathcal{X}). \end{aligned}$$

Because the covariance matrix factorises as  $\mathbf{K}_{b_{\mathbf{r}}, h} = \mathbf{B}_{\mathbf{r}, h} \mathbf{K}_{e, h} \mathbf{B}_{\mathbf{r}, h}$ , where  $\mathbf{K}_{e, h}$  is the covariance matrix for  $k_e$  at  $X_n^h$  and  $\mathbf{B}_{\mathbf{r}, h}$  is a diagonal matrix with entries  $b_{\mathbf{r}}(h\mathbf{x}_i)$ , we get

$$\mathcal{J}_n^h(\mathbf{r}) \leq 2 \sum_{i=1}^n \log \frac{b_{\mathbf{r}_0}(h\mathbf{x}_i)}{b_{\mathbf{r}}(h\mathbf{x}_i)} + \|\bar{f}\|_{\mathcal{H}_{k_{b_{\mathbf{r}_0}}}}^2(\mathcal{X}).$$

Then, since the class of error bounds  $b_{\mathbf{r}}$  is monotonically parametrised,  $\mathcal{J}_n^h(\mathbf{r}) \rightarrow -\infty$  as  $h \rightarrow 0$  uniformly over  $\mathbf{r} \in [\mathbf{0}, \mathbf{r}_0 - \boldsymbol{\epsilon}]$  for any  $\boldsymbol{\epsilon} > \mathbf{0}$ . Because  $\mathcal{J}_n^h(\mathbf{r}_0) = 0$ , this establishes that  $\liminf_{h \rightarrow 0} \mathbf{r}_n^h[f] \geq \mathbf{r}_0$ , as claimed.  $\square$

## B.10 Calculations for Multidimensional Output

To simplify the presentation we assume throughout that  $\sigma = 1$ , since  $\sigma$  enters only as a multiplicative constant that can be propagated through the calculations at the end. Let  $k_{\mathcal{X}}(\mathbf{x}, \mathbf{x}') := k_0^2 + b(\mathbf{x})b(\mathbf{x}')k_e(\mathbf{x}, \mathbf{x}')$ . From the Kronecker decomposition  $\mathbf{K} = \mathbf{K}_{\mathcal{X}} \otimes \mathbf{K}_{\mathcal{T}}$  we have that

$$\mathbf{K}^{-1} = (\mathbf{K}_{\mathcal{X}}^{-1}) \otimes (\mathbf{K}_{\mathcal{T}}^{-1})$$

where from (16) we know that

$$\mathbf{K}_{\mathcal{X}}^{-1} = \mathbf{K}_b^{-1} - \mathbf{K}_b^{-1} \mathbf{1} (k_0^{-2} + \mathbf{1}^\top \mathbf{K}_b^{-1} \mathbf{1})^{-1} \mathbf{1}^\top \mathbf{K}_b^{-1}.$$

Let  $\mathbf{k}(\mathbf{x}, \mathbf{t})$  be the column vector with entries  $k((\mathbf{x}_i, \mathbf{t}_i), (\mathbf{x}, \mathbf{t}))$ , and analogously define  $\mathbf{k}_{\mathcal{X}}(\mathbf{x})$  and  $\mathbf{k}_{\mathcal{T}}(\mathbf{t})$  as the column vectors with respective entries  $k_{\mathcal{X}}(\mathbf{x}_i, \mathbf{x})$  and  $k_{\mathcal{T}}(\mathbf{t}_i, \mathbf{t})$ . In this notation we have also the Kronecker decomposition  $\mathbf{k}(\mathbf{x}, \mathbf{t}) = \mathbf{k}_{\mathcal{X}}(\mathbf{x}) \otimes \mathbf{k}_{\mathcal{T}}(\mathbf{t})$  and the algebraic result that  $\mathbf{k}(\mathbf{x}, \mathbf{t})^\top = (\mathbf{k}_{\mathcal{X}}(\mathbf{x})^\top) \otimes (\mathbf{k}_{\mathcal{T}}(\mathbf{t})^\top)$ . For the conditional mean function we therefore have that

$$\begin{aligned} m_n[f](\mathbf{x}, \mathbf{t}) &= \mathbf{k}(\mathbf{x}, \mathbf{t})^\top \mathbf{K}^{-1} f(X_n) \\ &= [(\mathbf{k}_{\mathcal{X}}(\mathbf{x})^\top) \otimes (\mathbf{k}_{\mathcal{T}}(\mathbf{t})^\top)] [(\mathbf{K}_{\mathcal{X}}^{-1}) \otimes (\mathbf{K}_{\mathcal{T}}^{-1})] f(X_n) \\ &= [\mathbf{k}_{\mathcal{X}}(\mathbf{x})^\top \mathbf{K}_{\mathcal{X}}^{-1}] \otimes [\mathbf{k}_{\mathcal{T}}(\mathbf{t})^\top \mathbf{K}_{\mathcal{T}}^{-1}] f(X_n) \end{aligned}$$

where in the final equality we have exploited the *mixed-product* property of the Kronecker product. The dependence on  $k_0^2$  of this expression occurs only in the term  $\mathbf{k}_{\mathcal{X}}(\mathbf{x})^\top \mathbf{K}_{\mathcal{X}}^{-1}$ . From the calculations in Appendix B.2, we can take the  $k_0^2 \rightarrow \infty$  limit of the term  $\mathbf{k}_{\mathcal{X}}(\mathbf{x})^\top \mathbf{K}_{\mathcal{X}}^{-1}$ , to obtain that

$$m_n[f](\mathbf{x}, \mathbf{t}) = \left\{ \mathbf{k}_b(\mathbf{x})^\top \mathbf{K}_b^{-1} + [1 - \mathbf{k}_b(\mathbf{x})^\top \mathbf{K}_b^{-1} \mathbf{1}] \frac{\mathbf{1}^\top \mathbf{K}_b^{-1}}{\mathbf{1}^\top \mathbf{K}_b^{-1} \mathbf{1}} \right\} \otimes [k_{\mathcal{T}}(\mathbf{t})^\top \mathbf{K}_{\mathcal{T}}^{-1}] f(X_n).$$

For the conditional covariance function, we have from a similar argument based on the mixed-product property that

$$\begin{aligned} k_n[f]((\mathbf{x}, \mathbf{t}), (\mathbf{x}', \mathbf{t}')) &= k((\mathbf{x}, \mathbf{t}), (\mathbf{x}', \mathbf{t}')) - \mathbf{k}(\mathbf{x}, \mathbf{t})^\top \mathbf{K}^{-1} \mathbf{k}(\mathbf{x}', \mathbf{t}') \\ &= k_{\mathcal{X}}(\mathbf{x}, \mathbf{x}') k_{\mathcal{T}}(\mathbf{t}, \mathbf{t}') - \underbrace{[\mathbf{k}_{\mathcal{X}}(\mathbf{x})^\top \mathbf{K}_{\mathcal{X}}^{-1} \mathbf{k}_{\mathcal{X}}(\mathbf{x}')] [\mathbf{k}_{\mathcal{T}}(\mathbf{t})^\top \mathbf{K}_{\mathcal{T}}^{-1} \mathbf{k}_{\mathcal{T}}(\mathbf{t}')] }_{(*)}. \end{aligned} \quad (26)$$

The term  $(*)$  can be read off from (15) and (17):

$$(*) = (k_0^2 \mathbf{1} + \mathbf{k}_b(\mathbf{x}))^\top \left\{ \mathbf{K}_b^{-1} - \frac{\mathbf{K}_b^{-1} \mathbf{1} \mathbf{1}^\top \mathbf{K}_b^{-1}}{k_0^{-2} + \mathbf{1}^\top \mathbf{K}_b^{-1} \mathbf{1}} \right\} (k_0^2 \mathbf{1} + \mathbf{k}_b(\mathbf{x}'))$$

The fractional term can again be treated using the Taylor expansion (18) for  $k_0^{-2}$  at 0, which upon expanding brackets yields

$$(*) = \underbrace{k_0^2 + \mathbf{k}_b(\mathbf{x})^\top \mathbf{K}_b^{-1} \mathbf{k}_b(\mathbf{x}') - \frac{[\mathbf{k}_b(\mathbf{x})^\top \mathbf{K}_b^{-1} \mathbf{1} - 1][\mathbf{k}_b(\mathbf{x}')^\top \mathbf{K}_b^{-1} \mathbf{1} - 1]^\top}{\mathbf{1}^\top \mathbf{K}_b^{-1} \mathbf{1}}}_{(**)} + O(k_0^{-2}).$$

Substituting this expression into (26), and using the definition of  $k_{\mathcal{X}}$ , we obtain that

$$\begin{aligned} k_n[f]((\mathbf{x}, \mathbf{t}), (\mathbf{x}', \mathbf{t}')) &= (k_0^2 + k_b(\mathbf{x}, \mathbf{x}')) k_{\mathcal{T}}(\mathbf{t}, \mathbf{t}') - (k_0^2 + (**)) [\mathbf{k}_{\mathcal{T}}(\mathbf{t})^\top \mathbf{K}_{\mathcal{T}}^{-1} \mathbf{k}_{\mathcal{T}}(\mathbf{t}')] \\ &= k_0^2 \underbrace{[k_{\mathcal{T}}(\mathbf{t}, \mathbf{t}') - \mathbf{k}_{\mathcal{T}}(\mathbf{t})^\top \mathbf{K}_{\mathcal{T}}^{-1} \mathbf{k}_{\mathcal{T}}(\mathbf{t}')] }_{(***)} \\ &\quad + k_b(\mathbf{x}, \mathbf{x}') k_{\mathcal{T}}(\mathbf{t}, \mathbf{t}') - (***) [\mathbf{k}_{\mathcal{T}}(\mathbf{t})^\top \mathbf{K}_{\mathcal{T}}^{-1} \mathbf{k}_{\mathcal{T}}(\mathbf{t}')] \end{aligned}$$

where for  $\mathbf{t}, \mathbf{t}'$  in the training set we have  $(***) = 0$ , which gives the desired result.

## C Details for the Cardiac Model

This appendix summarises the most important aspects of the cardiac model that we used, and is principally intended for researchers working in the area of cardiac modelling who are interested in understanding the technical modelling aspects of the case study that we report in Section 3.

**Geometry** The model was based on a heart geometry obtained from a computer tomography (CT) dataset of a single patient, used in Strocchi et al. (2020, 2023). The original patient geometry was recorded using an average mesh resolution of  $1.06 \pm 0.16$  mm; below we describe how our coarser and finer meshes were constructed. Fibres in the atria and the ventricles were generated with *universal atrial coordinates* (Roney et al., 2019) and a rule-based method developed by Bayer et al. (2012). Full details about the geometry are provided in Strocchi et al. (2020, 2023).

**Atrial and Ventricular Activation** For the cardiac dynamics, we simulated atrial and ventricular activation using an *Eikonal model* (Neic et al., 2017)

$$\begin{aligned}\sqrt{\nabla t_a(\mathbf{x})^\top \mathbf{V}(\mathbf{x}) \nabla t_a(\mathbf{x})} &= 1 & \mathbf{x} \in \Omega \\ t_a(\mathbf{x}) &= t_0 & \mathbf{x} \in \Gamma\end{aligned}$$

where  $t_a(\mathbf{x})$  is the local activation time in the active domain  $\Omega$ ,  $\mathbf{V}$  is the tensor of the squared conduction velocities (CV) in the fibres, sheet and normal directions, and  $\Gamma$  is a subset of nodes in the domain that get activated at time  $t_0$ .

**Myocardium** The cardiac model that we used treats the myocardium as a transversely isotropic conduction medium. The fibre CV in the atrial and ventricular myocardium was set to 0.6 m/s and 0.9 m/s, consistent with experimental measurements (Taggart et al., 2000; Hansson et al., 1998), while the anisotropy ratio was set to 0.4 in all tissues (Strocchi et al., 2023). We simulated fast endocardial conduction in the ventricles by defining a 1 mm thick layer and assigning it with increased CV by five fold compared to normal ventricular myocardium (Ono et al., 2009). Fast conduction in the Bachmann bundle area in the atria was simulated by defining a region between the left and the right atrium as in Strocchi et al. (2023), and by assigning it with CV increased by 3.5 fold compared to normal atrial myocardium (Strocchi et al., 2023). The atria and ventricles were electrically isolated by defining an insulating layer to avoid non-physiological activation and to control the atrio-ventricular delay. Atrial and ventricular activation were initiated at the site of the right atrial and right ventricular pacing lead, respectively, identified from the CT images. The atrio-ventricular delay was set to 150 ms.

**Active Tension** Atrial and ventricular activation triggered a rise in local transmembrane potential (Neic et al., 2017), which then triggered a rise in active tension. Active tension was modelled with a phenomenological model developed by Niederer et al. (2011):

$$\begin{aligned}S_a(\mathbf{x}, t) &= T_{\text{peak}} \phi(\lambda) \tanh^2\left(\frac{t_s}{\tau_r}\right) \tanh^2\left(\frac{t_{\text{dur}} - t_s}{\tau_d}\right), & 0 < t_s < t_{\text{dur}}, \\ \phi(\lambda) &= \tan(\text{ld}(\lambda - \lambda_0)), & t_s = t - t_a(\mathbf{x}) - t_{\text{emd}}\end{aligned}$$

where  $T_{\text{peak}}$ ,  $\tau_r$ ,  $\tau_d$ ,  $t_{\text{dur}}$ ,  $\text{ld}$ ,  $\lambda_0$  and  $t_{\text{emd}}$  represent the reference tension, the rise and the decay time, the twitch duration, the reference stretch and the electro-mechanical delay. The following parameter values were used:

	$T_{\text{peak}}$ kPa	$\tau_r$ ms	$\tau_d$ ms	$t_{\text{dur}}$ ms	ld -	$\lambda_0$ -	$t_{\text{emd}}$ ms
<b>Atria</b>	80	100	50	450	0.7	6	20
<b>Ventricles</b>	60	50	50	200	0.7	6	20

**Passive Properties** We simulated passive properties of atrial and ventricular myocardium with a transversely isotropic Guccione law

$$\Psi(\mathbf{E}) = \frac{C}{2} [e^Q - 1],$$

$$Q = b_{\text{ff}} E_{\text{ff}}^2 + 2b_{\text{fs}} (E_{\text{fs}}^2 + E_{\text{fn}}^2) + b_{\text{ss}} (E_{\text{ss}}^2 + E_{\text{nn}}^2 + 2E_{\text{sn}}^2),$$

where f, s, n in the Cauchy–Green strain tensor  $\mathbf{E}$  represent the strain in the local fibres, sheet and normal to sheet directions, and  $C$ ,  $b_{\text{ff}}$ ,  $b_{\text{fs}}$ ,  $b_{\text{ss}}$  are the bulk stiffness, and the stiffness in the fibre, cross-fibre and transverse directions. The following parameter values were used:

	$C$ kPa	$b_{\text{ff}}$	$b_{\text{fs}}$	$b_{\text{ss}}$
<b>Atria</b>	3	25	11	9
<b>Ventricles</b>	4	25	11	9

Parameters in tissues other than the atria and the ventricles were represented with a neo-Hookean law and the parameters were set according to Strocchi et al. (2020, 2023). For all tissues, near-incompressibility was enforced with a penalty method with a bulk modulus  $\kappa = 1000.0$  kPa. To constrain the motion of the heart, we applied omni-directional springs on the superior vena cava and the two right pulmonary veins, as well as a region around the apex (Figure 5, left). Spring stiffness was set to 0.1 kPa/ $\mu\text{m}$ .

**Adjusting the Spatial Resolution** We used `meshtool`, open-source software for mesh manipulation (Neic et al., 2020), to refine or coarsen the mesh to a desired spatial resolution for the experiments that we report. The spatial resolution  $x_1$  that we used for extrapolation in the main text is the *nominal* resolution fed into `meshtool`, but we note that the nominal resolution is typically not exactly achieved in the re-meshing process; we therefore also report the effective average mesh resolution:

Target dx [mm]	Effective dx [mm]	# nodes	# elements
1.7	1.7	119,104	540,621
1.4	1.36	213,580	1,018,699
1.0	1.06	417,863	1,988,945
0.7	0.86	764,094	3,679,517
0.6	0.7	1,498,007	7,512,728
0.5	0.56	3,006,080	15,768,118
0.4	0.43	6,217,838	30,699,422

**Computational Resources** All simulations were carried out using the *Cardiac Arrhythmia Research Package* (CARP) (Vigmond et al., 2003; Augustin et al., 2021) on ARCHER2, a UK national super computing service (<https://www.archer2.ac.uk/>).